Tracking down hyper-boosted top quarks

Andrew J. Larkoski,[a] **Fabio Maltoni,**[b] **and Michele Selvaggi**[b]

[a] *Centre for Theoretical Physics, Massachusetts Institute of Technology, Cambridge, MA 02139, USA*

[b] *Centre for Cosmology, Particle Physics and Phenomenology (CP3), Université catholique de Louvain, Chemin du Cyclotron 2, B-1348 Louvain-la-Neuve, Belgium*

E-mail: larkoski@mit.edu, fabio.maltoni@uclouvain.be, michele.selvaggi@uclouvain.be

ABSTRACT: The identification of hadronically decaying heavy states, such as vector bosons, the Higgs, or the top quark, produced with large transverse boosts has been and will continue to be a central focus of the jet physics program at the Large Hadron Collider (LHC). At a future hadron collider working at an order-of-magnitude larger energy than the LHC, these heavy states would be easily produced with transverse boosts of several TeV. At these energies, their decay products will be separated by angular scales comparable to individual calorimeter cells, making the current jet substructure identification techniques for hadronic decay modes not directly employable. In addition, at the high energy and luminosity projected at a future hadron collider, there will be numerous sources for contamination including initial- and final-state radiation, underlying event, or pile-up which must be mitigated. We propose a simple strategy to tag such "hyper-boosted" objects that defines jets with radii that scale inversely proportional to their transverse boost and combines the standard calorimetric information with charged track-based observables. By means of a fast detector simulation, we apply it to top quark identification and demonstrate that our method efficiently discriminates hadronically decaying top quarks from light QCD jets up to transverse boosts of 20 TeV. Our results open the way to tagging heavy objects with energies in the multi-TeV range at present and future hadron colliders.

Contents

1 Introduction

The discovery of the Higgs boson [1, 2] represents a landmark in the exploration of the electroweak scale started with Run I of the LHC. The forthcoming Run II will extend the energy frontier for the direct searches further into the multi-TeV range, providing the first data that will test the up-to-now complete Standard Model (SM) to higher energies and to higher degree of precision. Among the best probes available to study the electroweak scale and the underlying mechanism responsible for its breaking are the vector bosons, the Higgs, and the top quark. Because of their large masses with respect to the electroweak scale, this implies a "strong" interaction with the Higgs field and therefore possibly enhanced couplings to new resonances and a higher sensitivity to deviations from SM predictions. In particular, the heavy states in the SM are responsible for large radiative corrections to the Higgs mass leading to the hierarchy problem. New physics models that solve the hierarchy problem and feature states at multi-TeV scales therefore will presumably significantly couple to heavy bosons and the top quark.

This sensitivity to new physics makes the efficient identification of vector bosons, the Higgs, and the top quark an important goal for the LHC and future colliders. Two simple factors need to be taken into account in the quest for the optimal tagging strategies. The first is that the largest decay rates of all the electroweak heavy states of the SM are into hadronic final states, producing multiple jets. For instance, the top quark features a two-body (semi-weak) decay into a b quark and a W boson, the latter decaying to a jet pair

around 67% of the time. For the Higgs boson the branching ratio into jets approaches 80%. The inability to select and identify such objects when decaying hadronically would therefore severely limit the final statistics available for physics studies. The second factor is that all methods for identification and the relevant backgrounds are highly sensitive to the p_T of the heavy state. For example, top quarks produced near threshold decay to widely-separated and relatively low p_T jets, with dominant backgrounds from multi-jet production in QCD. This low-p_T regime presents significant challenges, both because QCD backgrounds can be enormous and because the combinatorics of determining the set of jets which came from a single top quark decay can be very inefficient. The same argument applies to the heavy bosons of the SM.

At moderate boosts, with p_T up to a few times the heavy state mass, the decay products begin to merge, and become collimated in the detector. In this regime, combinatoric ambiguities and QCD backgrounds are greatly reduced. All jets produced from the decay of a heavy state can be clustered into the same jet, with a large jet radius, and so backgrounds are limited to high-p_T jets in QCD which have masses around that of the heavy state. Further, one can study the substructure of the fat jets to identify prongy structure that would be a signature of a decay, and be highly unlikely in a QCD jet. With this motivation, the past several years have seen substantial development and implementation of observables for identifying boosted hadronically decaying heavy objects produced at the LHC [3–5]. Several of the most powerful techniques have been validated on data [6–28] and are now standard tools for jet analysis at ATLAS and CMS.

Both because of the relatively low boosts and the fine granularity of the detectors, techniques for identifying heavy states at the LHC have impressive performance by exploiting all of the radiation from an event. However, looking forward to Run II of the LHC and beyond, many of the techniques used thus far will be significantly limited for several reasons. First, at higher luminosities there are more secondary proton collisions (pile-up) that contaminate the primary hard collision event. Tracking can be used to identify the charged particles that originated from the hard collision, but observables that depend on calorimetry will be significantly degraded by pile-up contamination. Grooming the jet [29–39] to remove that radiation that most likely came from pile-up will be required. Also, as the centre-of-mass energy of the LHC increases, more heavy bosons and top quarks at higher transverse momenta will be created. With a transverse momentum of a few TeV, the decay products begin to merge into a single calorimeter cell with the current resolution of ATLAS and CMS. At higher transverse momenta, unless the angular granularity increases significantly, using the calorimeter for identification of weak-scale particles will be essentially impossible. In this "hyper-boosted" regime, where p_Ts approach and exceed 10 TeV, it may be possible to access multi-boson/multi-top signatures such as VVV, $t\bar{t}H/V$, four top quarks, or even more exotic final states. Such final states produce huge numbers of low p_T jets and it would to be extremely difficult to reconstruct the individual heavy states, separate them from background, or resolve combinatorics.

With the recent excitement for a long-term goal of a 100 TeV future circular collider (FCC) [40–42], both of these issues become more acute. For example, at such high collision energies, weak bosons and the top quark could be produced with transverse momenta of

Process	Cross section at pp, $\sqrt{s} = 100$ TeV		
	$p_T > 1$ TeV (pb)	$p_T > 5$ TeV (fb)	$p_T > 10$ TeV (ab)
Standard Model — Signals — $pp \to t\bar{t}$	12	2.8	24
$pp \to t\bar{t}j$	52	14	94
$pp \to tj$	0.67	0.46	0.76
$pp \to t\bar{t}V$	0.40	0.30	3.7
$pp \to t\bar{t}H$	0.19	7.4e-02	0.65
$pp \to t\bar{t}t\bar{t}$	0.17	8.5e-02	0.51
Bkgds — $pp \to jj$	3500	1000	11000
$pp \to jjV$	110	130	2200
BSM — $pp \to Z' \to t\bar{t}$ ($m_{Z'} = 3$ TeV)	4.6	-	-
$pp \to Z' \to t\bar{t}$ ($m_{Z'} = 15$ TeV)	7.1e-03	4.7	-
$pp \to Z' \to t\bar{t}$ ($m_{Z'} = 30$ TeV)	7.1 e-05	6.5e-02	48
$pp \to \tilde{t}\tilde{t} \to t\bar{t} + \not{E}_T$ ($m_{\tilde{t}} = 1$ TeV)	0.49	7.8e-03	-
$pp \to \tilde{t}\tilde{t} \to t\bar{t} + \not{E}_T$ ($m_{\tilde{t}} = 5$ TeV)	7.5e-04	0.063	-
$pp \to \tilde{t}\tilde{t} \to t\bar{t} + \not{E}_T$ ($m_{\tilde{t}} = 10$ TeV)	4.4e-06	0.27e-03	0.024
$pp \to \tilde{g}\tilde{g} \to t\bar{t}t\bar{t} + \not{E}_T$ ($m_{\tilde{g}} = 2$ TeV)	2.5	0.94	-
$pp \to \tilde{g}\tilde{g} \to t\bar{t}t\bar{t} + \not{E}_T$ ($m_{\tilde{g}} = 5$ TeV)	2.7e-02	1.5	11
$pp \to \tilde{g}\tilde{g} \to t\bar{t}t\bar{t} + \not{E}_T$ ($m_{\tilde{g}} = 10$ TeV)	1.9e-04	0.12	4.5

Table 1: Inclusive leading-order cross sections for Standard Model and beyond-Standard Model (BR = 1) processes with at least one top quark with $p_T > 1$, 5, 10 TeV at a 100 TeV future collider. For the Standard Model backgrounds, the momentum requirement is imposed on one of the jets. Omitted entries have cross sections which are too small to be relevant.

order 10 TeV, with decay products separated by angles much smaller than the resolution of any foreseeable (sufficiently compact) calorimeter. To be more concrete, in Table 1, we collect representative inclusive cross sections for several SM and beyond-SM (BSM) processes at a 100 TeV collider calculated to leading order. With very strong p_T cuts on jets in the final state, backgrounds of jets from QCD can be dramatically reduced, while probing heavy mass resonances. For example, the decay of a SM-like Z' of 15 TeV to top quarks (assuming a branching fraction equal to 1) would produce about 5 events per fb^{-1} at 100 TeV with $p_T > 5$ TeV, while the dominant background, from $pp \to jj$ events, produces about 1000 events per fb^{-1}. Further predictions at next-to-leading order in QCD for cross sections with final state W, Z, H bosons and top quarks can found in Ref. [43].

The 100 TeV collider is projected to run at luminosities that are orders of magnitude greater than the LHC and so pileup will be a huge issue and grooming techniques will need to be understood at transverse momenta well beyond their current range of validity.

In addition, even resolving these issues, for a QCD jet with large transverse momentum, a perturbative emission can affect the jet mass by hundreds of GeV, comparable to the electroweak scale. The mass of a jet of radius $R \simeq 1$ and transverse momentum p_T is approximately given by

$$m^2 \simeq p_T \, p_T^{\text{soft}} R^2 \ , \tag{1.1}$$

where p_T^{soft} is the transverse momentum of a soft emission clustered in the jet. For example, at transverse momenta of $p_T \gtrsim 6$ TeV, an emission of only $p_T^{\text{soft}} = 5$ GeV would contribute to the jet mass an amount greater than the mass of the top quark.

Therefore, to push identification of electroweak-scale states to higher and higher energies requires controlling all of these effects. In this paper, we propose a new method as a robust and relatively p_T-independent procedure for identifying heavy SM states at very high boosts produced at a future collider and apply it to the case of the top quark. Our approach to boosted object discrimination at very high p_T consists of combining three elements:

I. **Global-jet calorimetric information**
   We are interested in the extreme limit where the energy deposit of a jet is confined to a single, or only a few, calorimetric cells. We assume that the information on the total energy of the jet (possibly determined also using the track information as in a particle-flow algorithm [44]) is available, but detailed information about the energy distribution inside the jet is not.

II. **Inner-jet charged track information**
   We exploit the high angular resolution of the tracking system to define observables sensitive to the internal structure of the jet only using charged particle tracks.

III. **Dynamic contamination removal**
   Contamination from initial state radiation (ISR), underlying event (UE) and pile-up is proportional to area of the jet. In addition for a coloured particle such as the top quark, for a fixed jet radius more perturbative QCD radiation is emitted as the p_T increases and is collected by the jet algorithm. Such an effect degrades the accuracy of the jet mass reconstruction and therefore the efficiency of tagging the boosted object. On the other hand, the typical angular size of a jet generated by a particle of mass m scales as m/p_T, i.e., inversely proportional to the transverse momentum. To mitigate all these effects we propose use of a jet radius that scales inversely with the jet p_T. This is similar to the variable R jet algorithm [45], with the important difference that in our method the clustering metric is not modified.

To develop and test our identification strategy, we employ DELPHES [46, 47], a modular and fast detector simulation framework. With DELPHES, we are able to make qualitative, and (thanks to especially designed modifications/improvements) to some extent also quantitative statements about finite resolution effects on the final discrimination power.

This paper is organised as follows. In Sec. 2, we introduce the methods and observables used for the identification of heavy state jets at very high p_T explicitly applied to the case

of a top quark. In addition to identifying top quarks through the jet invariant mass reconstruction, we measure N-subjettiness and energy correlation function observables to identify the substructure characteristic of a top quark decay. In Sec. 3, we apply our top quark finding procedure to a single jet p_T range, presenting a detailed analysis and comparison between LHC detectors and projected performance of detectors in a future collider. We also show that, even in the hyper-boosted regime, top quark identification efficiencies can be 40%, while rejecting over 90% of the dominant background. We draw our conclusions and discuss the outlook of tagging hyper-boosted objects in Sec. 4. Appendices provide details of the DELPHESfast detector simulation used throughout this paper and plots of top tagging results for a wide range of jet p_T.

2 Observables and methodology

In this section, we introduce the methods and observables that we will use throughout this paper to identify boosted hadronically decaying states. While the approach is quite general and, as it will be clear in the following, could be applied to tag other heavy states such as colour-singlet bosons, in this work we will focus on top quark identification.

2.1 Jet finding and definition

For a given jet radius R, the angular size of the top quark decay products scales as m_{top}/p_T and therefore significantly shrinks as the p_T increases. On the other hand even in the absence of pile-up, the amount of radiation in the event, both from the initial and final state, generically increases with the jet p_T. Our aim will be to show that mitigating both initial- and final-state radiation effects can be efficiently achieved by dynamically scaling the jet radius by the jet p_T.

Because the top quark is unstable, final-state radiation (FSR) arises from two possible sources: either before it decays, or from the the daughter bottom quark after the decay.[1] Ideally, for an optimal invariant mass reconstruction, the former type of radiation should not be clustered into the top quark jet while the latter should. At low p_Ts, radiation from top quark is suppressed, as it must vanish when the top is at rest. This is a general property of QCD (and QED) radiation from any massive particle that often phrased in terms of a dead cone: radiation about the direction of motion of the top quark is suppressed in a cone of angular size m_{top}/p_T; see Fig. 1. As the momentum of the top quark increases, the dead-cone shrinks and more phase space opens up for radiation from the top quark.

The contribution from ISR (or UE) to the p_T of the jet scales like R^2 (proportional to the area of the jet) while the effect on the squared mass scales like R^4 because ISR is approximately uncorrelated with final state jets. At very high transverse momenta, ISR will

---

[1]We remind the reader that the notion of initial- and final-state radiation and that of associating emissions to individual coloured particles is an approximation valid only in the collinear limit in the narrow-width approximation. For the top quark, the notion of radiation before or after its decay is meaningful when $1/E_{\text{rad}} \simeq \tau_{\text{rad}} < \tau_{\text{top}} = 1/\Gamma_{\text{top}}$, where E_{rad} is the characteristic energy scale of the radiation. By contrast, for a colour-singlet like the W boson, radiation from its decay products are localised about the direction of the W, in a region scaling like the characteristic angular size of the decay, m_W/p_T.
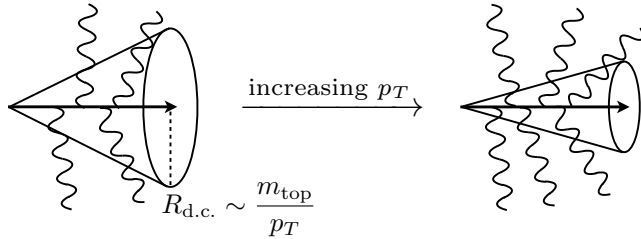
Figure 1: Illustration of the dead-cone effect. Final-state radiation from a top quark is suppressed within an angular region scaling like $R_{\text{d.c.}} \sim m_{\text{top}}/p_T$, called the dead-cone region. As the p_T of the top quark increases, the amount of radiation emitted from the top quark in a fixed angular region increases both due to the increase in energy and the decrease in size of the dead-cone region.

only distort the p_T spectrum of the jets slightly, but can affect the jet mass substantially. To see this behavior, consider a top quark jet of radius R with a single emission near the boundary of the jet. As long as the energy of this emission is small with respect to the energy of the top, its effect on the jet mass m is approximately given by

$$m^2 \simeq m_{\text{top}}^2 + p_T\, p_T^{\text{ISR}} R^2 \;. \tag{2.1}$$

Therefore, an ISR emission in the jet can contribute a mass comparable to the mass of the top quark when

$$p_T^{\text{ISR}} \simeq \frac{m_{\text{top}}^2}{p_T R^2} \;. \tag{2.2}$$

At moderate boosts, typical of the LHC, where $p_T \sim$ few $\times m_{\text{top}}$, ISR of 50 GeV or so can affect the jet mass by an $\mathcal{O}(1)$ amount (with $R \sim 1$). While this is quite hard radiation at the LHC, its effect must be mitigated in top quark mass measurements; numerous methods have been introduced to groom jets so as to remove contaminating radiation in the jet [29–39]. However, at the ranges of p_Ts accessible by a future collider, the jet p_T can be several to tens of TeV. In this regime, even emissions of a few GeV can change the jet mass by an $\mathcal{O}(1)$ amount. Thus, it is absolutely necessary to consider these effects at a future collider.

One is therefore lead to consider whether grooming methods that have been successfully applied at the LHC to mitigate contamination from both FSR and ISR could be applied at higher energies and luminosities. So far the standard grooming techniques have not been studied in detail in such an extreme environment[2] and so we will consider an alternative (simpler and possibly more robust) approach.

To this aim, we note that the ISR effects scale like the jet radius to a positive power and the dead-cone effect suppresses FSR in a region of angular size m_{top}/p_T. We can therefore reduce the contamination from radiation by appropriately scaling the jet radius by (the inverse of) its p_T. The specific procedure that we employ for boosted top quarks

---

[2]Some studies of extreme pile-up or jet grooming at energies and luminosities beyond current LHC applications are [27, 28, 48–50].

is the following. We first find jets with the anti-k_T algorithm [51] and the Winner-Take-All (WTA) recombination scheme [50, 52–54] with a fixed jet radius, which we take to be $R = 1.0$. We then recluster the jet with the anti-k_T algorithm where we set the subjet radius to:

$$R = C \frac{m_{\text{top}}}{p_T} \, , \tag{2.3}$$

where C is a constant and p_T is defined by the original, fixed-radius, jet. We then keep only the hardest subjet found with this procedure and promote it to be the boosted top quark jet. With this prescription, the resulting jet is parametrically affected by contamination from ISR as

$$m^2 \simeq m_{\text{top}}^2 + p_T \, p_T^{\text{ISR}} \left(\frac{C \, m_{\text{top}}}{p_T} \right)^2$$

$$\simeq m_{\text{top}}^2 \left(1 + C^2 \frac{p_T^{\text{ISR}}}{p_T} \right) \, , \tag{2.4}$$

whose effects are suppressed by the (small) ratio p_T^{ISR}/p_T. Similarly, because we choose the jet radius to scale with jet p_T, the dead-cone effect suppresses contamination from FSR over a fraction of the area of the jet that is independent of jet p_T. To ensure that the scaled radius jet captures the decay products of the top quark, in the remainder of the paper, we will adopt $C = 4$, corresponding to including above 95% of the energy fraction of the top quark decay products.[3] We note that this coefficient should be optimised in an actual analysis. However, as our aim is to illustrate the principle, we prefer to choose a conservative value so to be sure to cluster as much radiation from the top quark decay products as possible.

This approach is similar to variable R jets [45] in which the clustering metric for the k_T class of algorithms [51, 56–60] is modified to be

$$d_{ij} = \min[p_{Ti}^{2n}, p_{Tj}^{2n}] R_{ij}^2 \, , \qquad\qquad d_{iB} = p_{Ti}^{2n} \frac{\rho^2}{p_{Ti}^2} \, , \tag{2.5}$$

where ρ is a dimensionful constant. The beam distance d_{iB} sets the effective jet radius to scale inversely with the p_T of the jet. In contrast to variable R jets, our procedure does not modify the jet algorithm. Because we first find a fat jet and then recluster to find the hardest subjet, our procedure effectively defines an infrared and collinear (IRC) safe seeded cone jet algorithm with a radius that scales inversely with p_T.

2.2 Track-based observables

Scaling the jet radius inversely with p_T decreases the amount of contamination radiation in the jet, though it does so at the cost of reducing the number of calorimeter cells in the detector that contribute to the jet. As a consequence, the calorimetric angular resolution is also reduced, though this effect was to be expected anyway because the angular size of the decay products decreases as the p_T increases. Here, we explore recovering high

---

[3]Ref. [55] proposed a shrinking cone algorithm with a radius determined by the demanding that a fixed fraction of final state radiation was captured into the jet.
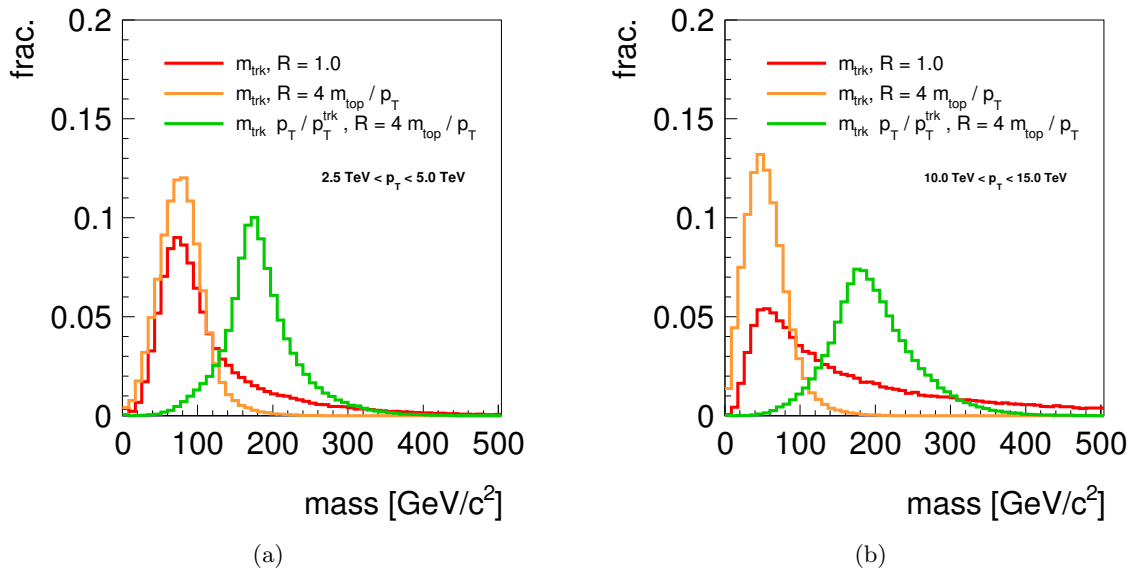
Figure 2: Distributions of the jet mass defined in three different ways in two p_T bins: $2-5$ TeV (left) and $10-15$ TeV (right). The red curves are the mass of jets with radius $R = 1.0$ measured on tracks; orange curves are the mass of jets with scaled radius $R = 4m_{\text{top}}/p_T$ measured on charged tracks; green curves are the track mass of jets rescaled by the ratio of total jet p_T to the p_T of tracks with the scaled jet radius $R = 4m_{\text{top}}/p_T$.

angular resolution by measuring jet observables from charged particle tracks. We propose to use standard calorimetric information (together with tracks in the case of particle-flow algorithms) to determine the total energy of the jet and use tracking information only for its substructure. For observables like the jet mass, when measured on tracks, this systematically biases the mass to lower values because charged particles do not contain the full energy of the jet. However, the bulk of this bias can be removed and the jet mass restored to its "nominal" value by simply rescaling the track-based mass by the ratio of the total jet p_T to the p_T of its charged tracks.[4] That is, in this paper we define the reconstructed jet mass as

$$m = \frac{p_T}{p_T^{\text{tracks}}} m_{\text{tracks}}, \qquad (2.6)$$

where m_{tracks} is the mass as measured on charged tracks and p_T^{tracks} is the transverse momentum of the tracks. We will also compare observables measured on current and projected future calorimetry to the track-based measurements.

In Fig. 2, we plot the top quark jet mass distribution measured on charged tracks to illustrate the effectiveness of our procedure, for two jet energy ranges. For these plots, we have simulated $pp \to t\bar{t}$ at leading order at 100 TeV center-of-mass energy with the MadGraph5_aMC@NLO 2.2.2 [64], Pythia 6.4 [65, 66] and Delphes 3.1.2 simulation

---

[4]We thank Gavin Salam for suggesting this procedure. A related technique was employed in the charged-track version of the HEPTopTagger [61, 62] of Ref. [63].

chain. Jets are clustered with FASTJET 3.0.6 [67] using the anti-k_T algorithm and WTA recombination scheme. We identify the jet in the event with the largest p_T that lies in the appropriate bin. We plot results corresponding to three different jet mass definitions: the track jet mass measured on jets with fixed jet radius $R = 1.0$, the track jet mass measured on jets with radius that scales with p_T as described earlier, and the rescaled track jet mass defined in Eq. (2.6). Both bare track jet masses are, as expected, systematically smaller than the true top quark mass. As the jet p_T increases from a few TeV to over 10 TeV, the track mass as measured on fixed-radius jets significantly drifts to higher values, due to the increased contamination from ISR/FSR. On the other hand, the rescaled track mass measured on the scaled-radius jet peaks around the top quark mass, independent of the jet p_T bin.

While the measurement of the jet mass is certainly a key observable to successfully identify a boosted top quark, it has to be kept in mind that large masses can also be generated by perturbative soft and collinear emissions in a QCD jet initiated by light quarks or gluons at high transverse momentum. In the collinear approximation, the average squared QCD jet mass is [68, 69]

$$\langle m^2 \rangle \simeq a_i \frac{\alpha_s}{\pi} p_T^2 R^2 \,, \tag{2.7}$$

where a_i is a constant that depends on the jet algorithm and is proportional to the colour of the initiating parton. While this provides a rule-of-thumb for the location of the peak, the QCD jet mass distribution is very wide. Nevertheless, at sufficiently high p_T with a fixed jet radius, QCD jets can have masses comparable to and even exceeding that of the top quark. This approximately occurs when

$$m_{\text{top}}^2 \lesssim a_i \frac{\alpha_s}{\pi} p_T^2 R^2 \,, \tag{2.8}$$

or when $p_T \gtrsim 600$ GeV, assuming $R \simeq a_i/\pi \simeq 1$. Using our scaled jet radius procedure, the mass of QCD jets is instead modified to

$$\langle m^2 \rangle \simeq a_i \frac{\alpha_s}{\pi} C^2 m_{\text{top}}^2 \,, \tag{2.9}$$

independent of the jet p_T, but comparable to the mass of the top quark. Therefore a mass cut is not sufficient to efficiently reduce QCD backgrounds, and observables that are independent of the jet mass must be used.

Particularly sensitive observables for boosted top quark identification are those that measure the prongy-ness of the jet. QCD jets dominantly consist of a single hard core of radiation, while hadronically decaying top quark jets typically have a 3-prong substructure. Several such observables have been proposed and studied [3–5]. In this work we employ the N-subjettiness observables $\tau_N^{(\beta)}$ and the n-point energy correlation functions $e_n^{(\beta)}$. The N-subjettiness observables $\tau_N^{(\beta)}$ are defined as

$$\tau_N^{(\beta)} = \sum_{i \in J} p_{Ti} \min \left\{ R_{i1}^\beta, \ldots, R_{iN}^\beta \right\} \,, \tag{2.10}$$

where the sum runs over particles in the jet J, p_{Ti} is the transverse momentum of particle i with respect to the beam, and R_{iK} is the boost-invariant angle between particle i and subjet axis K, and $\beta > 0$ is an angular exponent whose value can be used to control sensitivity to wide-angle radiation. In our study, we use the exclusive k_T algorithm [56] with the WTA recombination scheme on the jet to define the N subjet axes. For the identification of 3-prong top quark jets, it has been shown [70, 71] that the ratio

$$\tau_{3,2}^{(\beta)} = \frac{\tau_3^{(\beta)}}{\tau_2^{(\beta)}},\tag{2.11}$$

is an efficient observable for top quark identification and is widely used in both ATLAS and CMS experiments. In our analysis, we will measure $\tau_{3,2}^{(\beta)}$ using only track information and on jets with a scaled jet radius, as described in Sec. 2.1.

The (dimensionless) n-point energy correlation functions are defined as (for $n = 2, 3, 4$) [72]:

$$e_2^{(\beta)} = \frac{1}{p_T^2} \sum_{i<j \in J} p_{Ti}\, p_{Tj} R_{ij}^{\beta},$$

$$e_3^{(\beta)} = \frac{1}{p_T^3} \sum_{i<j<k \in J} p_{Ti}\, p_{Tj}\, p_{Tk}\, (R_{ij} R_{ik} R_{jk})^{\beta},$$

$$e_4^{(\beta)} = \frac{1}{p_T^4} \sum_{i<j<k<l \in J} p_{Ti}\, p_{Tj}\, p_{Tk}\, p_{Tl}\, (R_{ij} R_{ik} R_{il} R_{jk} R_{jl} R_{kl})^{\beta},\tag{2.12}$$

where R_{ij} is the boost invariant angle between particles i and j. Employing power counting of the soft and collinear regions of phase space, Ref. [73] showed that the particular combination

$$D_3^{(\alpha,\beta,\gamma)} \equiv \frac{e_4^{(\gamma)}\left(e_2^{(\alpha)}\right)^{\frac{3\gamma}{\alpha}}}{\left(e_3^{(\beta)}\right)^{\frac{3\gamma}{\beta}}} + x\frac{e_4^{(\gamma)}\left(e_2^{(\alpha)}\right)^{\frac{2\gamma}{\beta}-1}}{\left(e_3^{(\beta)}\right)^{\frac{2\gamma}{\beta}}} + y\frac{e_4^{(\gamma)}\left(e_2^{(\alpha)}\right)^{\frac{2\beta}{\alpha}-\frac{\gamma}{\alpha}}}{\left(e_3^{(\beta)}\right)^2},\tag{2.13}$$

for angular exponents α, β, γ is the optimal observable for identification of 3-prong jets formed from the energy correlation functions. Here,

$$x = \kappa_1 \left(\frac{(p_T^{\text{cut}})^2}{m_{\text{top}}^2}\right)^{\left(\frac{\alpha\gamma}{\beta}-\frac{\alpha}{2}\right)}, \quad y = \kappa_2 \left(\frac{(p_T^{\text{cut}})^2}{m_{\text{top}}^2}\right)^{\left(\frac{5\gamma}{2}-2\beta\right)},\tag{2.14}$$

where p_T^{cut} is a proxy for the p_T bin of the jet sample of interest. We will take $\kappa_1 = \kappa_2 = 1$ for simplicity in the following, keeping in mind that varying their values may provide improved discrimination. We will find that $\tau_{3,2}^{(\beta)}$ and $D_3^{(\alpha,\beta,\gamma)}$ are complementary observables for boosted top identification.

3 Detailed studies at fixed p_T

In this section, we present a detailed study of the methods introduced before in a restricted jet p_T range relevant for top quark identification at a future collider. The results quantify
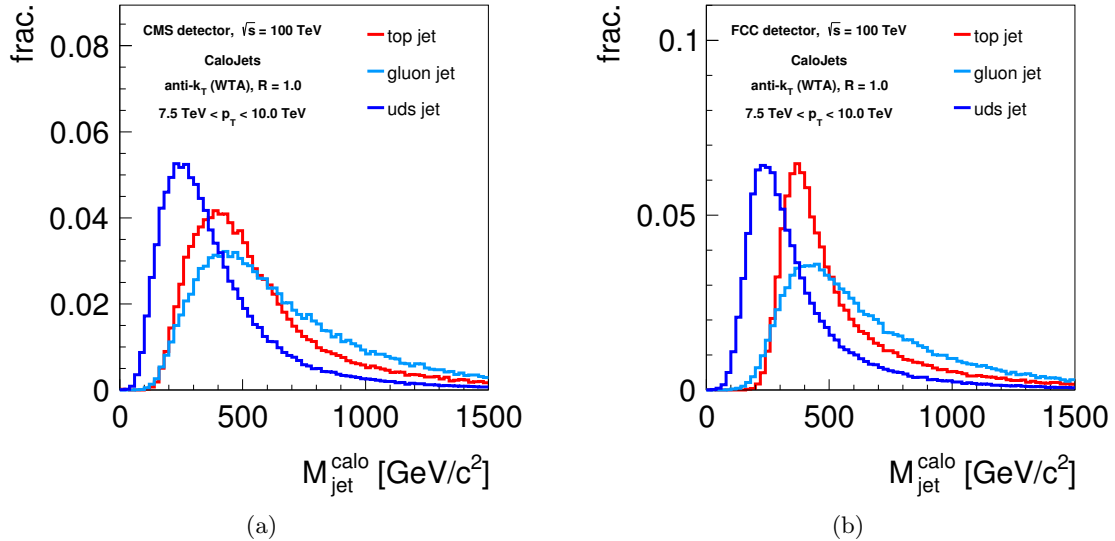
Figure 3: Distributions of the jet mass as measured on anti-k_T jets with radius $R = 1.0$ and $p_T \in [7.5, 10]$ TeV on boosted top jets and QCD jets from light quarks and gluons. (a) Mass distribution as measured from the CMS detector's calorimeter. (b) Mass distribution as measured from a future collider detector's calorimeter.

the discrimination power of our top quark tagging methods, show that projected calorimetry of a future collider is insufficient, and tracked-based information can provide the needed complementary information. App. B collects plots and analyses for a different set of jet p_T bins demonstrating that our arguments have a wide range of validity.

Here, we consider jets in the p_T range of $7.5 - 10$ TeV. The reason for this choice is the following. First, the p_T is sufficiently hard that standard methods show clear limitations. The angular size of the top quark decay products in this bin is approximately

$$R_{\text{top}} \sim \frac{2m_{\text{top}}}{p_T} \lesssim \frac{2 \cdot 175 \text{ GeV}}{7.5 \text{ TeV}} \approx 0.05 \,, \qquad (3.1)$$

which is comparable to the resolution of the electromagnetic calorimeters at ATLAS and CMS. Therefore, the reconstruction of top quark jets produced in this p_T bin will be very sensitive to the resolution of the detector and can provide a valuable benchmark for future collider detector resolution goals.

To do this, we will compare the efficiency to identify boosted top quark jets by using the standard calorimetric information only and by using our track-based method in a simulated CMS-like detector and in a projected future 100 TeV collider using DELPHES. The parameters for the fast detector simulation are presented in App. A and provide, we believe, rather conservative estimates for the resolution of detectors of a future collider. All event simulation is done with the MADGRAPH5_AMC@NLO 2.2.2, PYTHIA 6.4 and DELPHES 3.1.2 simulation chain. We study signal samples of boosted $Z' \to t\bar{t}$ events,
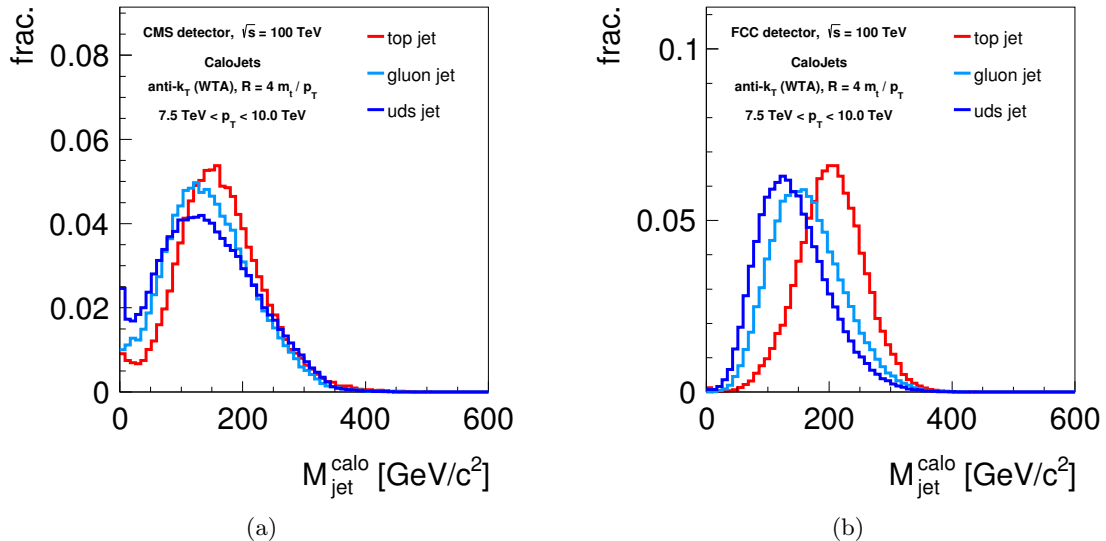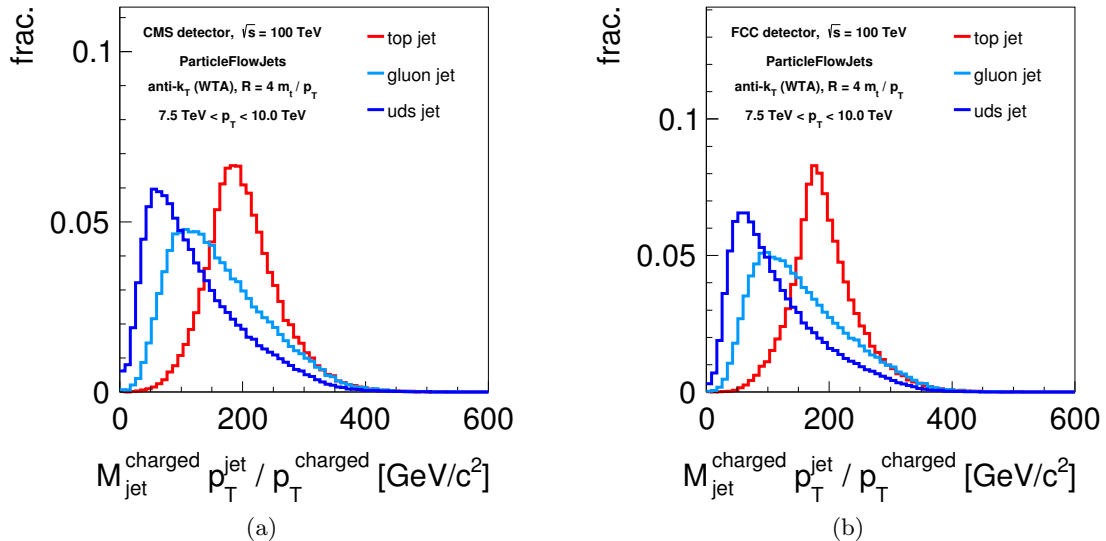
Figure 4: Distributions of the jet mass as measured on anti-k_T jets with radius $R = 4m_{\text{top}}/p_T$ and $p_T \in [7.5, 10]$ TeV on boosted top jets and QCD jets from light quarks and gluons. (a) Mass distribution as measured from the CMS detector's calorimeter. (b) Mass distribution as measured from a future collider detector's calorimeter.

where the mass of the Z' is varied depending on the p_T of the top quarks, and background samples of the partonic SM processes $q\bar{q} \to q'\bar{q}'$ and $gg \to gg$ at a 100 TeV pp collider. Jets are reconstructed using the anti-k_T algorithm with FastJet 3.0.6, with either a fixed jet radius or using the jet radius that scales with p_T, defined in Eq. (2.3). We ignore details and subtleties of defining quark flavor and gluon flavor jets, and pragmatically define them as what results from showering quark or gluon partons.

3.1 Mass Distributions

We begin by presenting the distribution for the jet mass in these samples as measured from calorimeter cells with a fixed jet radius $R = 1.0$. Distributions of the signal and background jet masses for the CMS and future collider detectors are presented in Fig. 3. Because of the large jet radius, there is a significant contamination from radiation in the jets, resulting in all mass distributions, either at CMS or a future collider, peaking at masses substantially greater than the top quark mass. Additionally, the light quark and gluon background distributions straddle the signal top quark distribution, showing that any background QCD jet sample would be essentially indistinguishable from a top quark sample from these mass distributions alone.

In Fig. 4, we present the distributions of the jet mass as measured on calorimeter jets with a scaled jet radius $R = 4m_{\text{top}}/p_T$. With the scaled jet radius, the amount of contamination in the jet is greatly reduced; however, the low resolution degrades the

Figure 5: Distributions of the rescaled track-based jet mass as measured on anti-k_T jets with radius $R = 4m_{\rm top}/p_T$ and $p_T \in [7.5, 10]$ TeV on boosted top jets and QCD jets from light quarks and gluons. (a) Distribution as measured from the CMS detector's tracking system. (b) Distribution as measured from a future collider detector's tracking system.

mass distributions measured in the CMS detector. Signal and background distributions overlap and all samples have a peak at zero mass indicating that the jet consists of a single calorimeter cell. Detector resolution effects are also significant in the mass distributions measured at a future collider. While the angular resolution of the calorimeter for the future collider scenario is $\times 2$ finer than for CMS (see App. A.2) and so these distributions do not have a peak at zero mass, the overlap of signal and background is substantial, and a cut on the mass would only result in a marginal top quark tagging efficiency.

Finally, in Fig. 5, we present the distributions of the jet mass as measured from tracks with the jet radius $R = 4m_{\rm top}/p_T$ and rescaling by the ratio of the total jet p_T to the track p_T. Unlike the jet mass as measured from the calorimeter, the rescaled track mass accurately reproduces the top mass for both the CMS and future collider detectors and barely suffers from resolution effects. Additionally, the mass distributions of QCD backgrounds are pushed to small values, below the mass of the top quark for both detectors. A cut in a window around the top quark mass would therefore robustly and efficiently discriminate boosted top quark jets from the QCD background. Larger rejection of QCD background can be accomplished by measuring additional substructure observables on the jet.

3.2   Substructure observables

As mentioned earlier, a jet mass comparable to the mass of the top quark can be reconstructed in several ways: for signal, by the decay into hard subjets and no FSR radiation;

while for background by the emission of significant amounts of soft radiation in the jet. For improved rejection of the background, in addition to the mass determination, observables on the jet that are sensitive to the 3-prong substructure of the top decay must to be measured. We therefore consider N-subjettiness ratio $\tau_{3,2}^{(\beta)}$ and the energy correlation function ratio $D_3^{(\alpha,\beta,\gamma)}$. While a full study of the efficiency as a function of the angular exponents and other parameters in these observables may result in improved discrimination power, we choose to use the parameters for boosted top tagging as recommended by the original investigations. That is, we consider the observables

$$\tau_{3,2} \equiv \tau_{3,2}^{(\beta=1)} \,, \qquad\qquad D_3 \equiv D_3^{(\alpha=2,\beta=0.8,\gamma=0.6)} \,, \qquad\qquad (3.2)$$

as measured on jets, which lie in the rescaled track-based mass window $m_J \in [120, 250]$ GeV in the following. Even without optimisation of parameters, we find impressive signal to background efficiency rates for jets produced at a 100 TeV collider.

In Fig. 6, we present the distributions of $\tau_{3,2}$ and D_3 measured on signal and background jets. We only consider these observables as measured on tracks and with jet radius that scales inversely with p_T. Though we only measure on tracks, because both $\tau_{3,2}$ and D_3 are dimensionless, we do not rescale them by the ratio of the total jet p_T to the charged track p_T. Both $\tau_{3,2}$ and D_3 provide excellent separation of signal and background jet samples, and in a complementary way. For $\tau_{3,2}$, the top quark distribution overlaps with the light quark distribution more than it does with gluons, while for D_3 the opposite occurs. While we do not have a complete theoretical understanding of this behaviour, this suggests that simultaneous measurement of $\tau_{3,2}$ and D_3 on jets would provide further discrimination power, depending on the light quark and gluon composition of the background sample.

To emphasise the discrimination power provided by $\tau_{3,2}$ and D_3, in Fig. 7 we show signal versus background efficiency curves (ROC curves) produced by making a sliding cut in either observable. As we require jets to lie in the rescaled track mass window $m \in [120, 250]$, the efficiencies in Fig. 7 include the effect of the mass cut. As anticipated, measuring these observables on tracks provides significant improvement in discrimination power as compared to including calorimeter information alone. Depending on the quark or gluon composition of the background sample, $\tau_{3,2}$ or D_3 measured on tracks provides better discrimination power. For example, at a future collider in this p_T bin at 50% top quark jet efficiency, 83% of gluon jets can be rejected by cuts on the mass and $\tau_{3,2}$, while 94% of light quark jets can be rejected by a mass cut and D_3. Thus, these observables exhibit a nice complementarity in how they can reject QCD background.

We stress that for the distributions in Fig. 6 and their corresponding ROC curves in Fig. 7, no optimisation has been performed. These observables have been applied "out of the box", using the values for their parameters as recommended in the original studies. Therefore, it may be possible to substantially improve boosted top quark discrimination power by optimising the free parameters that enter the definition of the observables. Nevertheless, even with this naïve application of a cut on the track mass and cuts on $\tau_{3,2}$ or D_3 impressive discrimination can be obtained. Additionally, while $\tau_{3,2}$ and D_3 are both sensitive to the 3-prong substructure, their relative performance rejecting gluon and light quark
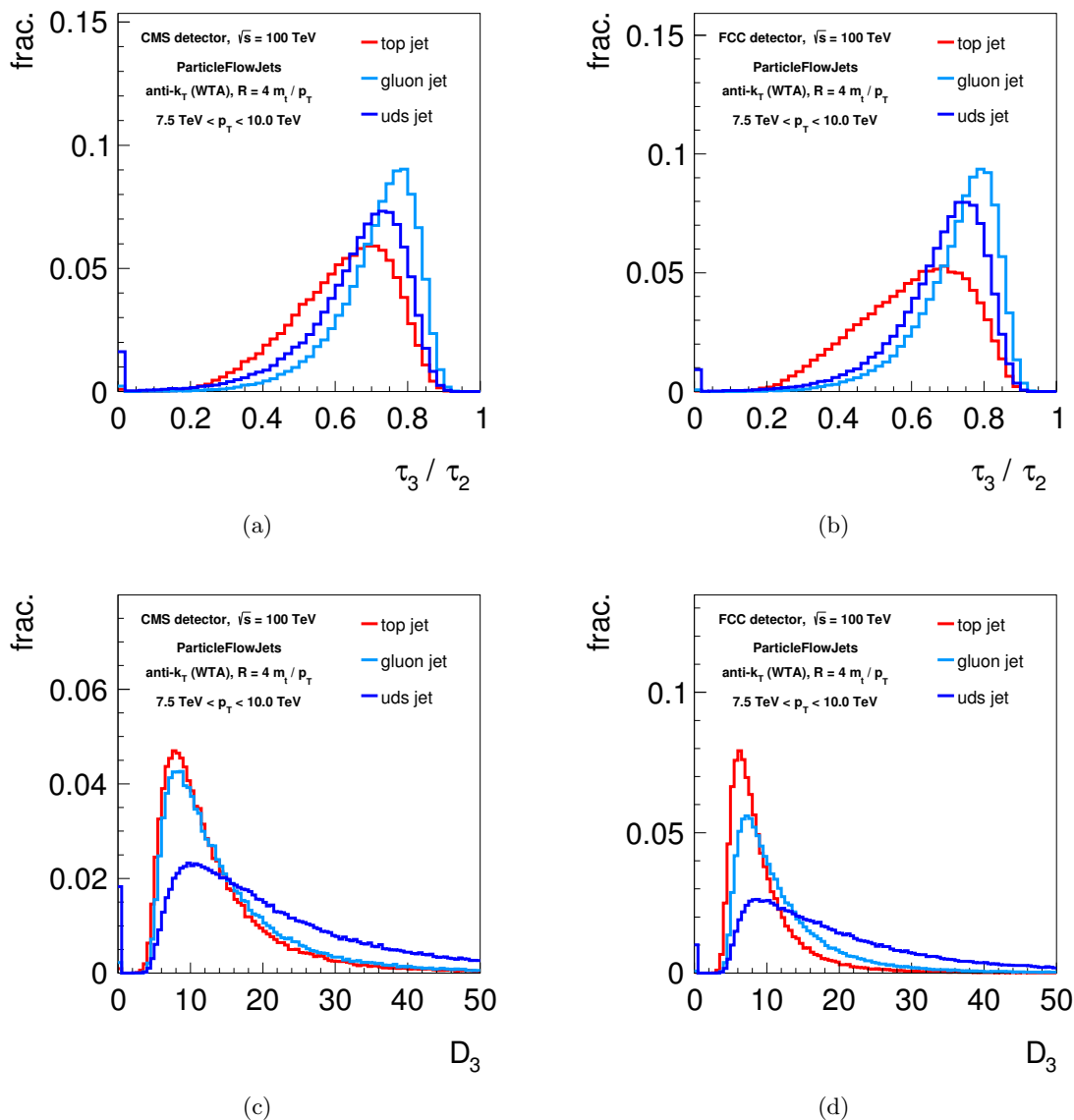
Figure 6: Distributions of the jet τ_3/τ_2 (top) and D_3 (bottom) as measured on anti-k_T jets with radius $R = 4m_{\text{top}}/p_T$ and $p_T \in [7.5, 10]$ TeV on boosted top jets and QCD jets from light quarks and gluons. Additionally, we require that the rescaled track-based mass lie in the window $m \in [120, 250]$ GeV. (left) Distributions as measured from the CMS detector's tracking system. (right) Distributions as measured from a future collider detector's tracking system.

jets is not well understood. The motivation for constructing these observables relies on the behavior of QCD in the parametric soft and collinear limits. However, gluon and light quark jets are not parametrically different objects, and so, without detailed calculation, it may not be possible to understand the performance. Further complication for detailed

(a)

(b)

(c)

(d)
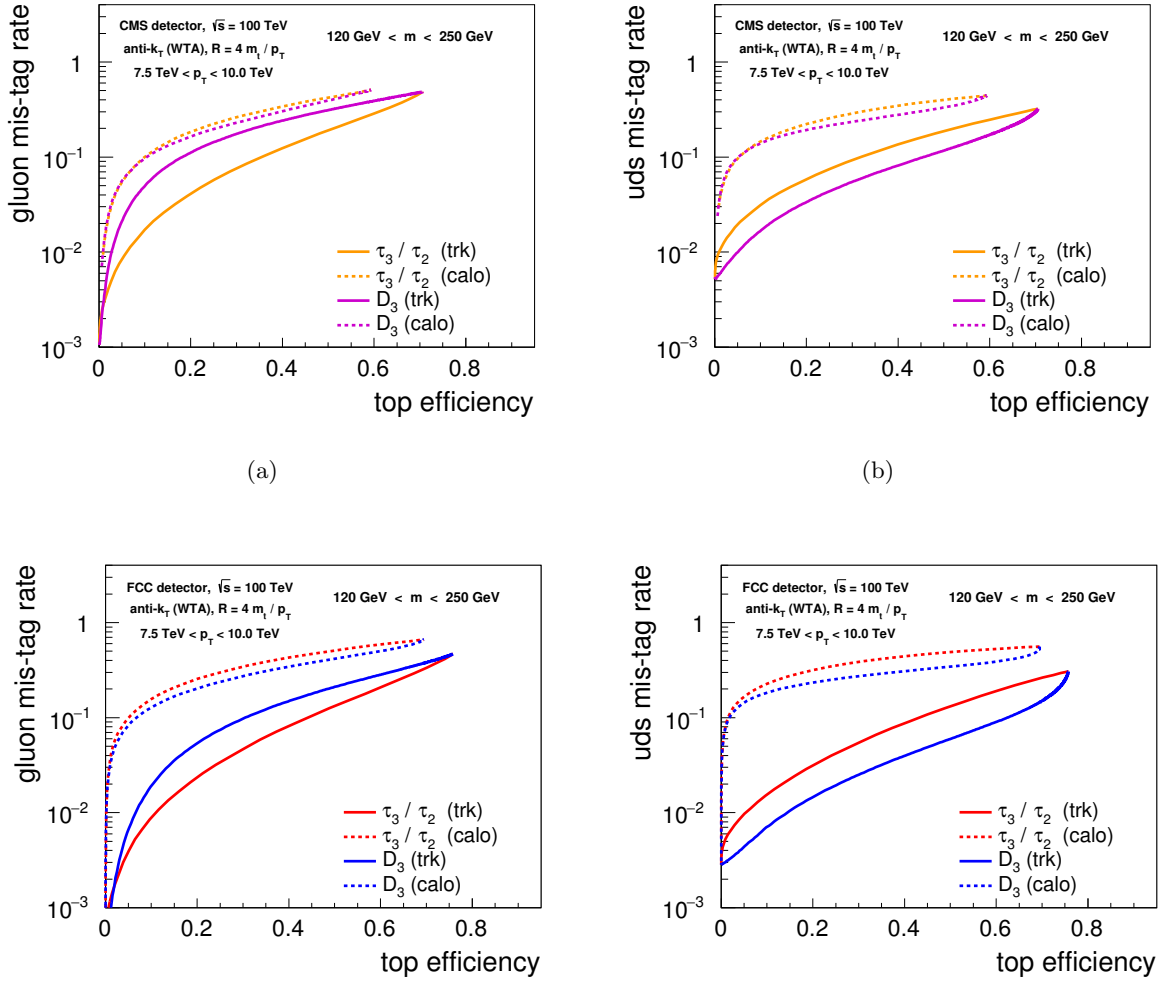
Figure 7: Signal vs. background efficiency (ROC) curves for top quark identification from QCD background utilising $\tau_{3,2}$ and D_3: (left) top quarks vs. gluon jets, (right) top quarks vs. light quark jets. The ROC curves as measured in the calorimeter are dashed lines and as measured on tracks are solid lines for (top) the CMS detector and (bottom) the FCC detector. The cut on the jet mass of $m \in [120, 250]$ GeV is included in the efficiencies.

theoretical understanding occurs because we only measure these observables on charged tracks. Quark and gluon partons fragment to charged hadrons differently, and this may also affect the discrimination power. A detailed study of these effects and their impact on discrimination power employing track-based methods of Refs. [74–76] would be certainly welcome, even though clearly beyond the scope of this paper.

4 Conclusions

We summarize the results of this paper in Fig. 8, illustrating the potential discrimination power for identifying boosted top quarks at the detector of a future high energy proton
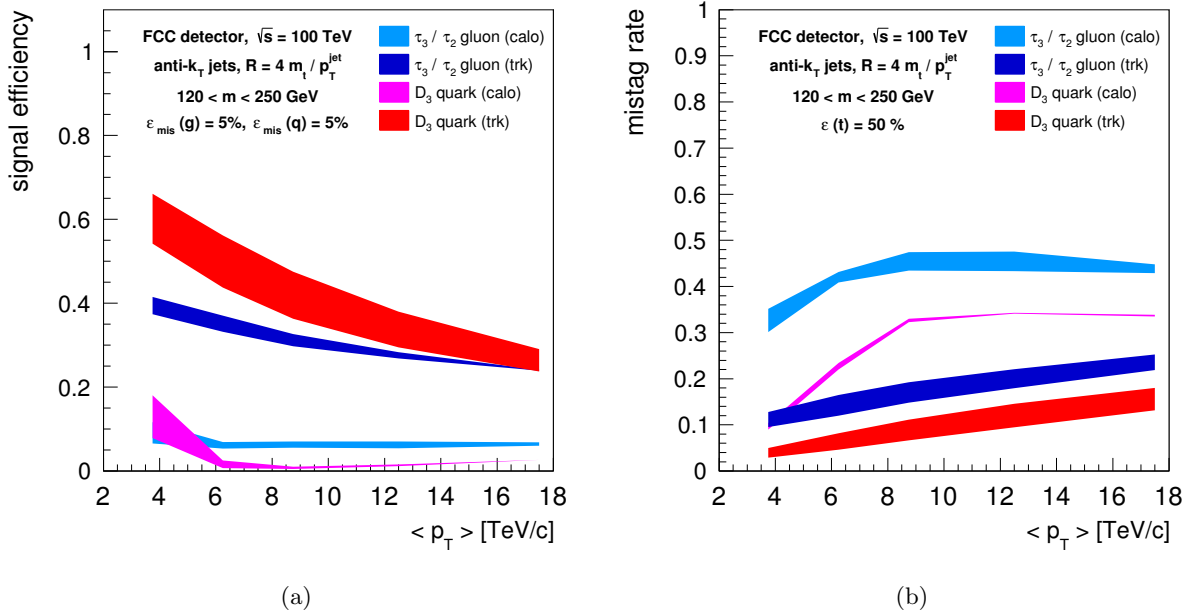
Figure 8: Plots illustrating the efficiency for tagging top quarks and rejecting QCD background as a function of jet p_T using tracking (blue, red) versus calorimetry (light blue, magenta) at a future collider. For identifying three-prong substructure the observables $\tau_{3,2}$ and D_3 have been used. (a) Top tagging efficiency for a fixed light quark and gluon mistag rate of 5%. (b) Light quark and gluon mistag rate at fixed top quark efficiency of 50%. The bands represent the envelope of efficiencies spanned by the Monte Carlo simulations (HERWIG 6 and PYTHIA 6.4) that we use.

collider modeled with DELPHES. On the left, we show the hadronically-decaying top quark tagging efficiency as a function of jet p_T at fixed mistag rate for jets produced from light quarks and gluons of 5% comparing our method using tracking versus using calorimetry exclusively. The bands represent the envelope of efficiencies from using either HERWIG 6 [77–79] or PYTHIA 6.4 Monte Carlo simulations. On the right, we plot the efficiency for mis-tagging jets initiated by light quarks or gluons as top quarks at fixed signal efficiency of 50%. Our procedure enables significant rejection rates at p_Ts approaching 20 TeV, while using calorimetry alone struggles to reject more background than signal. Exploiting tracking enables impressive signal efficiency, comparable to that of taggers used at the LHC, whose performance is relatively independent of jet p_T and extends well beyond 10 TeV.

In this paper, we have presented a procedure for the identification of top quarks in the multi-TeV energy range as those that could be produced at a future 100 TeV proton collider. High-resolution tracking information was required for identification of the prongs produced in the top quark decay and contamination due to initial- and final-state radiation, underlying event, pile-up, or other sources can be reduced significantly by dynamically

scaling the jet radius inversely proportional to the transverse momentum of the jets. By applying a simple jet selection on the track-based jet mass, N-subjettiness ratio, and energy correlation function based jet substructure observables, very high efficiency for discriminating boosted top quarks from light QCD jets can be accomplished, and with rates that are relatively independent of the boost. These results are encouraging for the prospects of precision studies of the electroweak sector at a future collider.

Though we have employed a fast detector simulation, we believe that the analysis presented here can provide a useful benchmark for performance and response of detectors at a future collider. The relatively conservative parameters in the fast detector simulation should provide a realistic goal for the resolution of a future detector. Nevertheless, there were several effects not included in this analysis. For example, we have not considered backgrounds to boosted top quarks from electroweak boson emission from light quarks. The main reason is that vector bosons in energetic jets are typically soft [80, 81] and therefore when decaying hadronically their effect is very similar to that of QCD radiation yet subleading due to the weak coupling. However, they may be relevant in high purity (low signal efficiency) samples. In addition, while rescaling the jet radius inversely proportional to the transverse momentum and using charged tracks reduces contamination from pile-up, we did not include any simulation of pile-up in our analysis. The effects of pile-up on the efficiency for tagging top quarks would be important to understand in a dedicated analysis, but we believe that the effects would be minimal because we use a recoil-free jet algorithm as well as scaling the jet radius.

Besides these experimental issues, our procedure for tagging highly boosted top quarks raises some interesting theoretical questions. Because of our prescription for scaling the jet radius, the angular size of the jets we consider becomes very small at sufficiently high transverse momenta. By restricting the radiation in the jet to such small angular regions, non-global logarithms [82], clustering logarithms [83], or logarithms of the jet radius itself [84–86] could become important for a theoretical understanding. For high angular resolution, we also require measurements on charged tracks, and not on all radiation in the jet. Therefore, a model of the fragmentation of partons to charged hadrons is required to predict the distributions of the jet substructure observables on these jets. An understanding of track-based observables [74–76] may also explain the difference that we observed between the performance of $\tau_{3,2}$ and D_3 on light quark or gluon jets and could potentially predict the optimal parameters of those observables for discrimination.

We also emphasize that the methods presented here apply more broadly than to top quarks alone. Studies for the identification of hyper-boosted 2-prong jets from hadronic decays of W, Z, or H bosons can benefit from these techniques. Contamination radiation can be controlled using the scaled jet radius, though, because these objects are colour-singlets and narrow resonances, unlike for top quarks, there is no contaminating FSR produced. Because the masses of the electroweak bosons are smaller than the top, using the high resolution of the tracker becomes even more important, as the structure of these jets lies at smaller angular scales. For identification of 2-prong substructure, instead of $\tau_{3,2}$ and D_3, one would use observables such as $\tau_{2,1}$ N-subjettiness ratio and D_2 formed from the energy correlation functions [87].

Looking forward to a future hadron collider during the era of the LHC provides context and motivation for collider physics studies in extreme environments. Additionally, analyses at the LHC itself can benefit from efforts for a future collider. For example, while the energies and luminosities at the LHC are an order of magnitude smaller than a proposed future collider, our proposal for jet radius rescaling and track-based measurements could be useful for analyses at the LHC in a high pile-up environment or over a large energy range. Looking forward to Run 2 at the LHC, a new, higher energy regime will be explored and will require the use of new techniques to push forward.

Acknowledgments

A   Parametrised detector simulation

The ability to disentangle the structure of jets is largely dependent on detector resolution effects, such as the angular and energy-momentum resolution of the jet constituents. In addition, the finite geometrical acceptance of the detector, and the presence of a magnetic field can have an influence on the measurement of jet properties. Such important detector effects have been taken into account by means of the fast simulation framework DELPHES [46]. For this study, two detector setups have been used: the CMS detector [88], as a reference for present performance, and a hypothetical detector for a future circular collider. The FCC detector measures particles created from pp collisions with $\sqrt{s} = 100$ TeV. Since no prototype of such a detector currently exists yet, the performance of existing detectors needs to be extrapolated to future scenarios. We will briefly describe the modeling of the detector response for these two configurations in this appendix.

A.1   Tracking

After collision, parton showering, hadronisation, and decays, the first step of DELPHESis the propagation of long-lived particles inside the tracking volume within a uniform axial magnetic field parallel to the beam direction. The magnetic field strength B, the size of the tracking radius L and the single hit spatial resolution $\sigma_{r\phi}$ are the main parameters that constrain the resolution on the track transverse momentum:

$$\frac{\sigma(p_T)}{p_T} \approx \frac{\sigma_{r\phi}}{B \cdot L^2} \, . \tag{A.1}$$
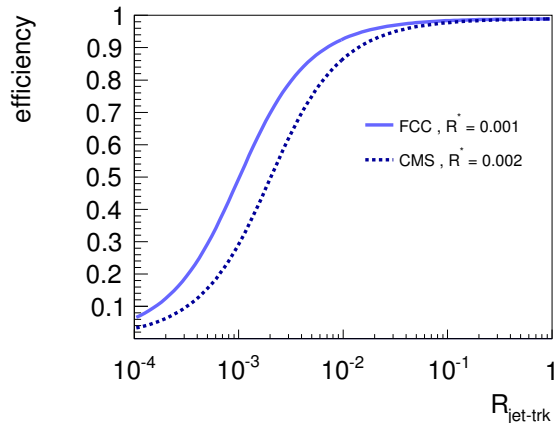
Figure 9: Tracking efficiency as a function of the transverse distance between the track direction and the jet center.

As a benchmark, we assume that the radius of the FCC inner detector is twice that of CMS and that the magnetic field is increased by a factor of $3/2$. We also assume that the spatial resolution $\sigma_{r\phi}$ is two times smaller than at CMS, which is possible by designing a more granular pixel detector [89]. These improvements in an FCC detector would allow measurements of 1 TeV charged hadrons with a precision of $\sigma(p_T)/p_T \simeq 1-2\%$.

In DELPHES, charged tracks are reconstructed assuming an infinite angular resolution, which is a good approximation for moderately boosted objects, but not optimal for the energy regime that is considered in this study. A module that performs a smearing on the track direction was therefore developed specifically for this study. We assume an overall factor 2 with respect to present CMS performance, which is mainly driven by a more granular detector, and can eventually improved further by increasing the number a tracker layers, which is possible thanks to a larger tracker volume. This leads to a conservative estimate for the angular resolution of the FCC tracker detector $\sigma(\theta, \phi) \simeq 10^{-3}$ rad.

Accounting for the finite angular resolution on the track direction is not enough in a high occupancy regime. Charged particles confined inside a highly boosted jet can be extremely collimated, resulting in unresolvable tracker hits, especially in the innermost tracking layers. Although an accurate description of this feature would require a full event reconstruction by means of a GEANT-based simulation [90], we construct a simple model of this effect by parametrising the track reconstruction efficiency as a function of the transverse distance between a track and the jet center. The jet center has the highest density of charged particles, and so this should describe the dominant effect on the resolution. For tracks a distance R from the jet center, we define the track resolution efficiency

$$\epsilon(R) = \frac{2\epsilon_0}{\pi} \arctan\left(\frac{R}{R^*}\right) , \tag{A.2}$$

which is plotted in Fig. 9.

	CMS	FCC
B_z (T)	3.8	6.0
Length (m)	6	12
Radius (m)	1.3	2.6
ϵ_0	0.90	0.95
R^*	0.002	0.001
$\sigma(p_T)/p_T$	$0.2 \cdot p_T$ (TeV/c)	$0.02 \cdot p_T$ (TeV/c)
$\sigma(\eta,\phi)$	0.002	0.001

Table 2: Tracking-related parameters for the CMS and FCC setup in Delphes.

	CMS	FCC
$\sigma(E)/E$ (ECAL)	$7\%/\sqrt{E} \oplus 0.7\%$	$3\%/\sqrt{E} \oplus 0.3\%$
$\sigma(E)/E$ (HCAL)	$150\%/\sqrt{E} \oplus 5\%$	$50\%/\sqrt{E} \oplus 1\%$
$\eta \times \phi$ cell size (ECAL)	(0.02×0.02)	(0.01×0.01)
$\eta \times \phi$ cell size (HCAL)	(0.1×0.1)	(0.05×0.05)

Table 3: Calorimeter parameters for the CMS and FCC setup in Delphes.

Inspired from CMS public tracker performance [91], we choose $\epsilon_0 = 90\%$ (95%) and $R^* = 0.002$ (0.001) for the CMS (FCC) detector. We stress that in principle the tracking angular resolution depends on the track momentum and pseudorapidity, but for simplicity we assume a constant (conservative) value. For a robust determination of the jet center in the case of light quarks and gluon jets we rely on the WTA recombination scheme. On the other hand, given that top quark jets often consists of three hard prongs, parametrising the efficiency as a function of the distance between the track and the jet center would result in an underestimate of track losses for tracks that belong to the subleading prongs. Therefore, in order to realistically simulate track losses inside top jets we first run the N-jettiness clustering algorithm [71, 92] at particle level to help us identify the three dominant subjet axes. We then require tracks to pass the efficiency criterion from Eq. (A.2) with respect to each subjet core. A summary of all the tracking parameters used for the tracking parametrisation in DELPHESis given in Table 2.

A.2 Calorimetry

After propagating within the magnetic field, long-lived particles reach the electromagnetic (ECAL) and hadronic (HCAL) calorimeters. Since these are modeled in DELPHESby two-dimensional grids of variable spacing, the calorimeter deposits natively include finite angular resolution effects. In order to accurately model the angular resolution on reconstructed jets, separate grids for ECAL and HCAL has been adopted for this study. The ECAL and HCAL maps for the CMS detector are taken from Ref. [88].

	p_T cut	[2.5, 5] TeV	[5, 7.5] TeV	[7.5, 10] TeV	[10, 15] TeV	[15, 20] TeV
		20% Top Efficiency				
gluons	CMS	2%	3%	4%	5%	6%
gluons	FCC	1%	2%	2%	3%	4%
quarks	CMS	1%	2%	3%	5%	7%
quarks	FCC	0.5%	1%	1.5%	2%	4%
		40% Top Efficiency				
	p_T cut	[2.5, 5] TeV	[5, 7.5] TeV	[7.5, 10] TeV	[10, 15] TeV	[15, 20] TeV
gluons	CMS	7%	9%	10%	14%	17%
gluons	FCC	5%	6%	7%	10%	12%
quarks	CMS	3%	5%	7%	11%	17%
quarks	FCC	1.5%	2.5%	4%	5%	8%
		60% Top Efficiency				
	p_T cut	[2.5, 5] TeV	[5, 7.5] TeV	[7.5, 10] TeV	[10, 15] TeV	[15, 20] TeV
gluons	CMS	18%	20%	24%	30%	38%
gluons	FCC	13%	15%	20%	24%	25%
quarks	CMS	7%	10%	15%	22%	30%
quarks	FCC	4%	6%	8%	11%	15%

Table 4: Table of background rejection rates at fixed signal efficiencies for jet p_Ts ranging from 2.5 TeV to 20 TeV at the CMS or FCC detector. For gluon (quark) jet backgrounds, efficiencies are determined from cuts on $\tau_{3,2}$ (D_3) measured on tracks. The cut on the rescaled track-based jet mass of $m_J \in [120, 250]$ GeV is included in the efficiencies.

For the FCC detector we assume that the same elementary calorimeter cells will be used, but placed at twice the CMS distance from the interaction point, leading to an improved angular resolution by a factor 2. In order to obtain the best possible energy resolution, the best nominal performance between the CMS [88] and ATLAS [93] calorimeters was chosen. The calorimeter performance for the CMS and FCC setups are summarised in Table 3.

B p_T scan and results

In this appendix, we present the results of our top quark identification procedure over a wide range of jet p_Ts at a 100 TeV future collider. A discussion of the physics or analysis of the results will be limited, as these were discussed in detail in the text. In Figs. 10, 11 and 12, we plot the jet mass, $\tau_{3,2}$ and D_3 distributions as measured on calorimeter jets with radius $R = 4m_{\rm top}/p_T$. As the jet p_T increases, finite resolution effects dominate, and especially in the CMS detector for jets in the highest p_T bin, a large fraction of the jets consist of a single calorimeter cell. In Figs. 13, 14 and 15, we plot the rescaled track-based mass, $\tau_{3,2}$ and D_3 distributions on charged tracks for jets with a radius $R = 4m_{\rm top}/p_T$ for

both signal and background jets. Figs. 16 and 17 show the signal vs. background efficiency curves for a simulated CMS or FCC detector, respectively, at a future 100 TeV collider. In these figures, we compare the discrimination power of the jet substructure observables $\tau_{3,2}$ and D_3 over a wide range of jet p_Ts as measured on calorimeter or track-based jets. As with the $p_T \in [7.5, 10]$ TeV bin studied in Sec. 3, discrimination power is significantly improved by working with track-based observables. In addition, $\tau_{3,2}$ is a better discriminant over a wide range of signal efficiencies than D_3 for background gluon jets, but the improvement decreases as p_T increases. D_3, on the other hand, is a much more powerful observable for rejecting light quark background jets than $\tau_{3,2}$. These features are further illustrated in Table 4 where we list the rejection rates ($= 100\% -$ background efficiency) for benchmark signal efficiencies, for jets with p_Ts ranging from 2.5 to 20 TeV.

References

[1] **ATLAS** Collaboration, G. Aad et al., *Observation of a new particle in the search for the Standard Model Higgs boson with the ATLAS detector at the LHC*, *Phys.Lett.* **B716** (2012) 1–29, [arXiv:1207.7214].

[2] **CMS** Collaboration, S. Chatrchyan et al., *Observation of a new boson at a mass of 125 GeV with the CMS experiment at the LHC*, *Phys.Lett.* **B716** (2012) 30–61, [arXiv:1207.7235].

[3] A. Abdesselam, E. B. Kuutmann, U. Bitenc, G. Brooijmans, J. Butterworth, et al., *Boosted objects: A Probe of beyond the Standard Model physics*, *Eur.Phys.J.* **C71** (2011) 1661, [arXiv:1012.5412].

[4] A. Altheimer, S. Arora, L. Asquith, G. Brooijmans, J. Butterworth, et al., *Jet Substructure at the Tevatron and LHC: New results, new tools, new benchmarks*, *J.Phys.* **G39** (2012) 063001, [arXiv:1201.0008].

[5] A. Altheimer, A. Arce, L. Asquith, J. Backus Mayes, E. Bergeaas Kuutmann, et al., *Boosted objects and jet substructure at the LHC. Report of BOOST2012, held at IFIC Valencia, 23rd-27th of July 2012*, *Eur.Phys.J.* **C74** (2014) 2792, [arXiv:1311.2708].

[6] **CMS** Collaboration, *Jet substructure algorithms*, Tech. Rep. CMS-PAS-JME-10-013, CERN, Geneva, 2011.

[7] **ATLAS** Collaboration, D. W. Miller, *Jet substructure in ATLAS*, Tech. Rep. ATL-PHYS-PROC-2011-142, 2011.

[8] **ATLAS** Collaboration, *Studies of the impact and mitigation of pile-up on large-r and groomed jets in atlas at $\sqrt{s} = 7$ tev*, Tech. Rep. ATLAS-CONF-2012-066, CERN, Geneva, Jul, 2012.

[9] **CMS** Collaboration, S. Chatrchyan et al., *Shape, transverse size, and charged hadron multiplicity of jets in pp collisions at 7 TeV*, *JHEP* **1206** (2012) 160, [arXiv:1204.3170].

[10] **ATLAS** Collaboration, G. Aad et al., *ATLAS measurements of the properties of jets for boosted particle searches*, *Phys.Rev.* **D86** (2012) 072006, [arXiv:1206.5369].

[11] **ATLAS** Collaboration, *Performance of large-r jets and jet substructure reconstruction with the atlas detector*, Tech. Rep. ATLAS-CONF-2012-065, CERN, Geneva, Jul, 2012.

[12] **ATLAS** Collaboration, G. Aad et al., *Jet mass and substructure of inclusive jets in $\sqrt{s} = 7$ TeV pp collisions with the ATLAS experiment*, *JHEP* **1205** (2012) 128, [arXiv:1203.4606].

[13] **ATLAS** Collaboration, G. Aad et al., *Performance of jet substructure techniques for large-R jets in proton-proton collisions at $\sqrt{s} = 7$ TeV using the ATLAS detector*, JHEP **1309** (2013) 076, [arXiv:1306.4945].

[14] **ATLAS** Collaboration, G. Aad et al., *Measurement of jet shapes in top pair events at sqrt(s) = 7 TeV using the ATLAS detector*, arXiv:1307.5749.

[15] **ATLAS** Collaboration, *Performance and Validation of Q-Jets at the ATLAS Detector in pp Collisions at $\sqrt{s}$=8 TeV in 2012*, Tech. Rep. ATLAS-CONF-2013-087, ATLAS-COM-CONF-2013-099, 2013.

[16] **ATLAS** Collaboration, *Jet Charge Studies with the ATLAS Detector Using $\sqrt{s} = 8$ TeV Proton-Proton Collision Data*, Tech. Rep. ATLAS-CONF-2013-086, ATLAS-COM-CONF-2013-101, 2013.

[17] **ATLAS** Collaboration, *Performance of pile-up subtraction for jet shapes*, Tech. Rep. ATLAS-CONF-2013-085, ATLAS-COM-CONF-2013-100, 2013.

[18] **ATLAS** Collaboration, *Pile-up subtraction and suppression for jets in ATLAS*, Tech. Rep. ATLAS-CONF-2013-083, ATLAS-COM-CONF-2013-097, 2013.

[19] **CMS** Collaboration, *Identifying Hadronically Decaying Vector Bosons Merged into a Single Jet*, Tech. Rep. CMS-PAS-JME-13-006, 2013.

[20] **CMS** Collaboration, *Performance of quark/gluon discrimination in 8 TeV pp data*, Tech. Rep. CMS-PAS-JME-13-002, 2013.

[21] **CMS** Collaboration, *Pileup Jet Identification*, Tech. Rep. CMS-PAS-JME-13-005, 2013.

[22] **CMS** Collaboration, *Measurement of the subjet multiplicity in dijet events from proton-proton collisions at sqrt(s) = 7 tev*, Tech. Rep. CMS-PAS-QCD-10-041, CERN, Geneva, 2010.

[23] **ATLAS** Collaboration, G. Aad et al., *Light-quark and gluon jet discrimination in pp collisions at $\sqrt{s} = 7$ TeV with the ATLAS detector*, arXiv:1405.6583.

[24] **ATLAS** Collaboration, P. Loch, *Studies of jet shapes and jet substructure in proton-proton collisions at $\sqrt{s} = 7$ TeV with ATLAS*, PoS **EPS-HEP2013** (2013) 442.

[25] **CMS** Collaboration, *Boosted Top Jet Tagging at CMS*, Tech. Rep. CMS-PAS-JME-13-007, 2014.

[26] **CMS** Collaboration, *V Tagging Observables and Correlations*, Tech. Rep. CMS-PAS-JME-14-002, 2014.

[27] **CMS** Collaboration, *Pileup Removal Algorithms*, Tech. Rep. CMS-PAS-JME-14-001, 2014.

[28] **ATLAS** Collaboration, *Tagging and suppression of pileup jets*, Tech. Rep. ATLAS-CONF-2014-018, ATLAS-COM-CONF-2014-025, 2014.

[29] J. M. Butterworth, A. R. Davison, M. Rubin, and G. P. Salam, *Jet substructure as a new Higgs search channel at the LHC*, Phys.Rev.Lett. **100** (2008) 242001, [arXiv:0802.2470].

[30] S. D. Ellis, C. K. Vermilion, and J. R. Walsh, *Techniques for improved heavy particle searches with jet substructure*, Phys.Rev. **D80** (2009) 051501, [arXiv:0903.5081].

[31] S. D. Ellis, C. K. Vermilion, and J. R. Walsh, *Recombination Algorithms and Jet Substructure: Pruning as a Tool for Heavy Particle Searches*, Phys.Rev. **D81** (2010) 094023, [arXiv:0912.0033].

[32] D. Krohn, J. Thaler, and L.-T. Wang, *Jet Trimming*, *JHEP* **1002** (2010) 084, [arXiv:0912.1342].

[33] G. Soyez, G. P. Salam, J. Kim, S. Dutta, and M. Cacciari, *Pileup subtraction for jet shapes*, *Phys.Rev.Lett.* **110** (2013), no. 16 162001, [arXiv:1211.2811].

[34] D. Krohn, M. D. Schwartz, M. Low, and L.-T. Wang, *Jet Cleansing: Pileup Removal at High Luminosity*, *Phys.Rev.* **D90** (2014), no. 6 065020, [arXiv:1309.4777].

[35] M. Dasgupta, A. Fregoso, S. Marzani, and G. P. Salam, *Towards an understanding of jet substructure*, *JHEP* **1309** (2013) 029, [arXiv:1307.0007].

[36] A. J. Larkoski, S. Marzani, G. Soyez, and J. Thaler, *Soft Drop*, *JHEP* **1405** (2014) 146, [arXiv:1402.2657].

[37] P. Berta, M. Spousta, D. W. Miller, and R. Leitner, *Particle-level pileup subtraction for jets and jet shapes*, *JHEP* **1406** (2014) 092, [arXiv:1403.3108].

[38] M. Cacciari, G. P. Salam, and G. Soyez, *SoftKiller, a particle-level pileup removal method*, *Eur.Phys.J.* **C75** (2015), no. 2 59, [arXiv:1407.0408].

[39] D. Bertolini, P. Harris, M. Low, and N. Tran, *Pileup Per Particle Identification*, *JHEP* **1410** (2014) 59, [arXiv:1407.6013].

[40] Y. Gershtein, M. Luty, M. Narain, L. T. Wang, D. Whiteson, et al., *Working Group Report: New Particles, Forces, and Dimensions*, arXiv:1311.0299.

[41] "Future circular collider study kick-off meeting." https://indico.cern.ch/event/282344/.

[42] "Workshop on future high energy circular colliders." http://indico.ihep.ac.cn/conferenceDisplay.py?confId=3813.

[43] P. Torrielli, *Rare Standard Model processes for present and future hadronic colliders*, arXiv:1407.1623.

[44] **CMS** Collaboration, *Particle-Flow Event Reconstruction in CMS and Performance for Jets, Taus, and MET*, .

[45] D. Krohn, J. Thaler, and L.-T. Wang, *Jets with Variable R*, *JHEP* **0906** (2009) 059, [arXiv:0903.0392].

[46] **DELPHES 3** Collaboration, J. de Favereau et al., *DELPHES 3, A modular framework for fast simulation of a generic collider experiment*, *JHEP* **1402** (2014) 057, [arXiv:1307.6346].

[47] M. Selvaggi, *DELPHES 3: A modular framework for fast-simulation of generic collider experiments*, *J.Phys.Conf.Ser.* **523** (2014) 012033.

[48] A. Avetisyan, J. M. Campbell, T. Cohen, N. Dhingra, J. Hirschauer, et al., *Methods and Results for Standard Model Event Generation at $\sqrt{s} = 14$ TeV, 33 TeV and 100 TeV Proton Colliders (A Snowmass Whitepaper)*, arXiv:1308.1636.

[49] J. Anderson, A. Avetisyan, R. Brock, S. Chekanov, T. Cohen, et al., *Snowmass Energy Frontier Simulations*, arXiv:1309.1057.

[50] A. J. Larkoski and J. Thaler, *Aspects of jets at 100 TeV*, *Phys.Rev.* **D90** (2014), no. 3 034010, [arXiv:1406.7011].

[51] M. Cacciari, G. P. Salam, and G. Soyez, *The Anti-k(t) jet clustering algorithm*, *JHEP* **0804** (2008) 063, [arXiv:0802.1189].

[52] D. Bertolini, T. Chan, and J. Thaler, *Jet Observables Without Jet Algorithms*, *JHEP* **1404** (2014) 013, [arXiv:1310.7584].

[53] A. J. Larkoski, D. Neill, and J. Thaler, *Jet Shapes with the Broadening Axis*, *JHEP* **1404** (2014) 017, [arXiv:1401.2158].

[54] G. Salam, *Unpublished, Unpublished.*

[55] Z. Han, *Jet Radiation Radius*, *Phys.Rev.* **D90** (2014), no. 7 074033, [arXiv:1402.1494].

[56] S. Catani, Y. L. Dokshitzer, M. Seymour, and B. Webber, *Longitudinally invariant K_t clustering algorithms for hadron hadron collisions*, *Nucl.Phys.* **B406** (1993) 187–224.

[57] S. D. Ellis and D. E. Soper, *Successive combination jet algorithm for hadron collisions*, *Phys.Rev.* **D48** (1993) 3160–3166, [hep-ph/9305266].

[58] Y. L. Dokshitzer, G. Leder, S. Moretti, and B. Webber, *Better jet clustering algorithms*, *JHEP* **9708** (1997) 001, [hep-ph/9707323].

[59] M. Wobisch and T. Wengler, *Hadronization corrections to jet cross-sections in deep inelastic scattering*, hep-ph/9907280.

[60] M. Wobisch, *Measurement and QCD analysis of jet cross-sections in deep inelastic positron proton collisions at $\sqrt{s} = 300$ GeV*, *DESY-THESIS-2000-049* (2000).

[61] T. Plehn, G. P. Salam, and M. Spannowsky, *Fat Jets for a Light Higgs*, *Phys.Rev.Lett.* **104** (2010) 111801, [arXiv:0910.5472].

[62] T. Plehn, M. Spannowsky, M. Takeuchi, and D. Zerwas, *Stop Reconstruction with Tagged Tops*, *JHEP* **1010** (2010) 078, [arXiv:1006.2833].

[63] S. Schaetzel and M. Spannowsky, *Tagging highly boosted top quarks*, *Phys.Rev.* **D89** (2014), no. 1 014007, [arXiv:1308.0540].

[64] J. Alwall, R. Frederix, S. Frixione, V. Hirschi, F. Maltoni, et al., *The automated computation of tree-level and next-to-leading order differential cross sections, and their matching to parton shower simulations*, *JHEP* **1407** (2014) 079, [arXiv:1405.0301].

[65] T. Sjostrand, S. Mrenna, and P. Z. Skands, *PYTHIA 6.4 Physics and Manual*, *JHEP* **0605** (2006) 026, [hep-ph/0603175].

[66] T. Sjostrand, S. Mrenna, and P. Z. Skands, *A Brief Introduction to PYTHIA 8.1*, *Comput.Phys.Commun.* **178** (2008) 852–867, [arXiv:0710.3820].

[67] M. Cacciari, G. P. Salam, and G. Soyez, *FastJet User Manual*, *Eur.Phys.J.* **C72** (2012) 1896, [arXiv:1111.6097].

[68] S. Ellis, J. Huston, K. Hatakeyama, P. Loch, and M. Tonnesmann, *Jets in hadron-hadron collisions*, *Prog.Part.Nucl.Phys.* **60** (2008) 484–551, [arXiv:0712.2447].

[69] G. P. Salam, *Towards Jetography*, *Eur.Phys.J.* **C67** (2010) 637–686, [arXiv:0906.1833].

[70] J. Thaler and K. Van Tilburg, *Identifying Boosted Objects with N-subjettiness*, *JHEP* **1103** (2011) 015, [arXiv:1011.2268].

[71] J. Thaler and K. Van Tilburg, *Maximizing Boosted Top Identification by Minimizing N-subjettiness*, *JHEP* **1202** (2012) 093, [arXiv:1108.2701].

[72] A. J. Larkoski, G. P. Salam, and J. Thaler, *Energy Correlation Functions for Jet Substructure*, *JHEP* **1306** (2013) 108, [arXiv:1305.0007].

[73] A. J. Larkoski, I. Moult, and D. Neill, *Building a Better Boosted Top Tagger*, *Phys.Rev.* **D91** (2015), no. 3 034035, [arXiv:1411.0665].

[74] W. J. Waalewijn, *Calculating the Charge of a Jet*, *Phys.Rev.* **D86** (2012) 094030, [arXiv:1209.3019].

[75] H.-M. Chang, M. Procura, J. Thaler, and W. J. Waalewijn, *Calculating Track-Based Observables for the LHC*, *Phys.Rev.Lett.* **111** (2013) 102002, [arXiv:1303.6637].

[76] H.-M. Chang, M. Procura, J. Thaler, and W. J. Waalewijn, *Calculating Track Thrust with Track Functions*, *Phys.Rev.* **D88** (2013) 034030, [arXiv:1306.6630].

[77] G. Marchesini, B. Webber, G. Abbiendi, I. Knowles, M. Seymour, et al., *HERWIG: A Monte Carlo event generator for simulating hadron emission reactions with interfering gluons. Version 5.1 - April 1991*, *Comput.Phys.Commun.* **67** (1992) 465–508.

[78] G. Corcella, I. Knowles, G. Marchesini, S. Moretti, K. Odagiri, et al., *HERWIG 6: An Event generator for hadron emission reactions with interfering gluons (including supersymmetric processes)*, *JHEP* **0101** (2001) 010, [hep-ph/0011363].

[79] G. Corcella, I. Knowles, G. Marchesini, S. Moretti, K. Odagiri, et al., *HERWIG 6.5 release note*, hep-ph/0210213.

[80] J. R. Christiansen and T. Sjstrand, *Weak Gauge Boson Radiation in Parton Showers*, *JHEP* **1404** (2014) 115, [arXiv:1401.5238].

[81] F. Krauss, P. Petrov, M. Schoenherr, and M. Spannowsky, *Measuring collinear W emissions inside jets*, *Phys.Rev.* **D89** (2014), no. 11 114006, [arXiv:1403.4788].

[82] M. Dasgupta and G. Salam, *Resummation of nonglobal QCD observables*, *Phys.Lett.* **B512** (2001) 323–330, [hep-ph/0104277].

[83] A. Banfi and M. Dasgupta, *Problems in resumming interjet energy flows with k_t clustering*, *Phys.Lett.* **B628** (2005) 49–56, [hep-ph/0508159].

[84] M. Seymour, *Jet shapes in hadron collisions: Higher orders, resummation and hadronization*, *Nucl.Phys.* **B513** (1998) 269–300, [hep-ph/9707338].

[85] E. Gerwick, S. Schumann, B. Gripaios, and B. Webber, *QCD Jet Rates with the Inclusive Generalized kt Algorithms*, *JHEP* **1304** (2013) 089, [arXiv:1212.5235].

[86] M. Dasgupta, F. Dreyer, G. P. Salam, and G. Soyez, *Small-radius jets to all orders in QCD*, arXiv:1411.5182.

[87] A. J. Larkoski, I. Moult, and D. Neill, *Power Counting to Better Jet Observables*, *JHEP* **1412** (2014) 009, [arXiv:1409.6298].

[88] **CMS** Collaboration, G. Bayatian et al., *CMS physics: Technical design report*, Tech. Rep. CERN-LHCC-2006-001, CMS-TDR-008-1, 2006.

[89] **CMS** Collaboration, A. Dominguez et al., *CMS Technical Design Report for the Pixel Detector Upgrade*, Tech. Rep. CERN-LHCC-2012-016, CMS-TDR-011, FERMILAB-DESIGN-2012-02, 2012.

[90] **GEANT4** Collaboration, S. Agostinelli et al., *GEANT4: A Simulation toolkit*, *Nucl.Instrum.Meth.* **A506** (2003) 250–303.

[91] **CMS** Collaboration, "High pt jets tracking." https://twiki.cern.ch/twiki/bin/view/CMSPublic/HighPtTrackingDP.

[92] I. W. Stewart, F. J. Tackmann, and W. J. Waalewijn, *N-Jettiness: An Inclusive Event Shape to Veto Jets*, Phys.Rev.Lett. **105** (2010) 092002, [arXiv:1004.2489].

[93] **ATLAS** Collaboration, G. Aad et al., *Expected Performance of the ATLAS Experiment - Detector, Trigger and Physics*, arXiv:0901.0512.
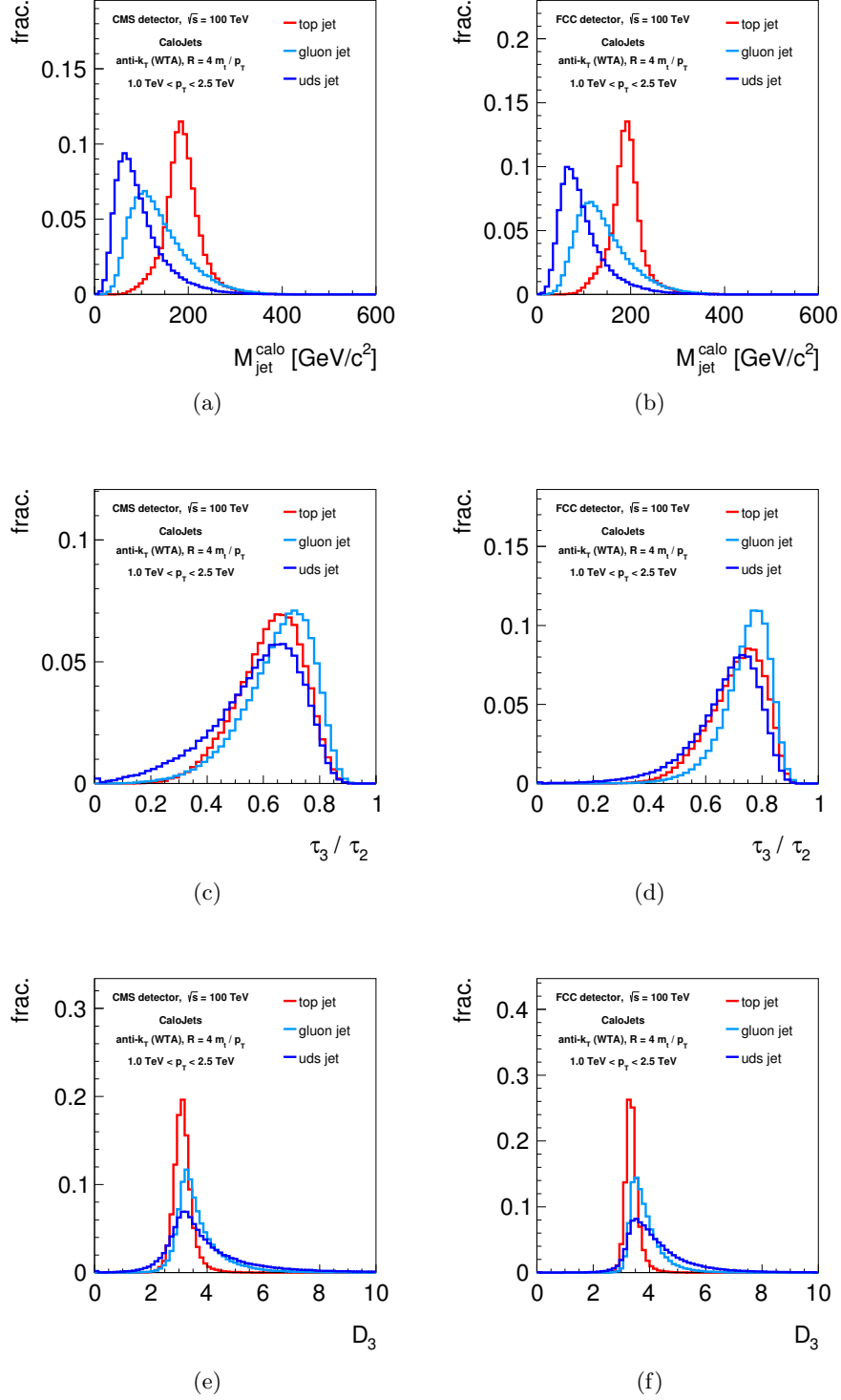
Figure 10: Distributions of the jet mass (top), τ_3/τ_2 (middle), and D_3 (bottom) as measured on anti-k_T jets with radius $R = 4m_{\text{top}}/p_T$ and $p_T \in [1.0, 2.5]$ TeV on boosted top jets and QCD jets from light quarks and gluons. (left) Distributions as measured from the CMS detector's calorimeter system. (right) Distributions as measured from a future collider detector's calorimeter system.
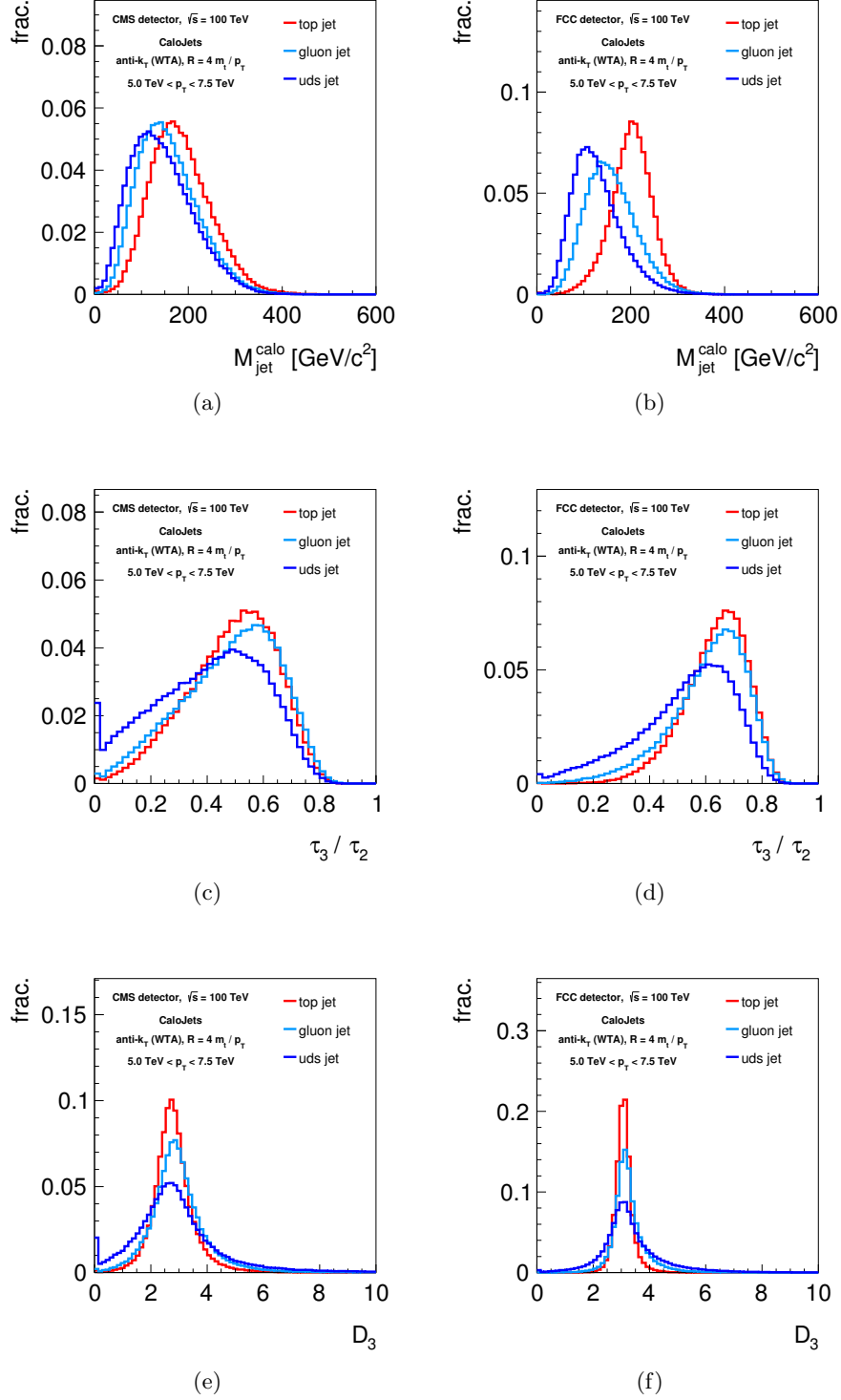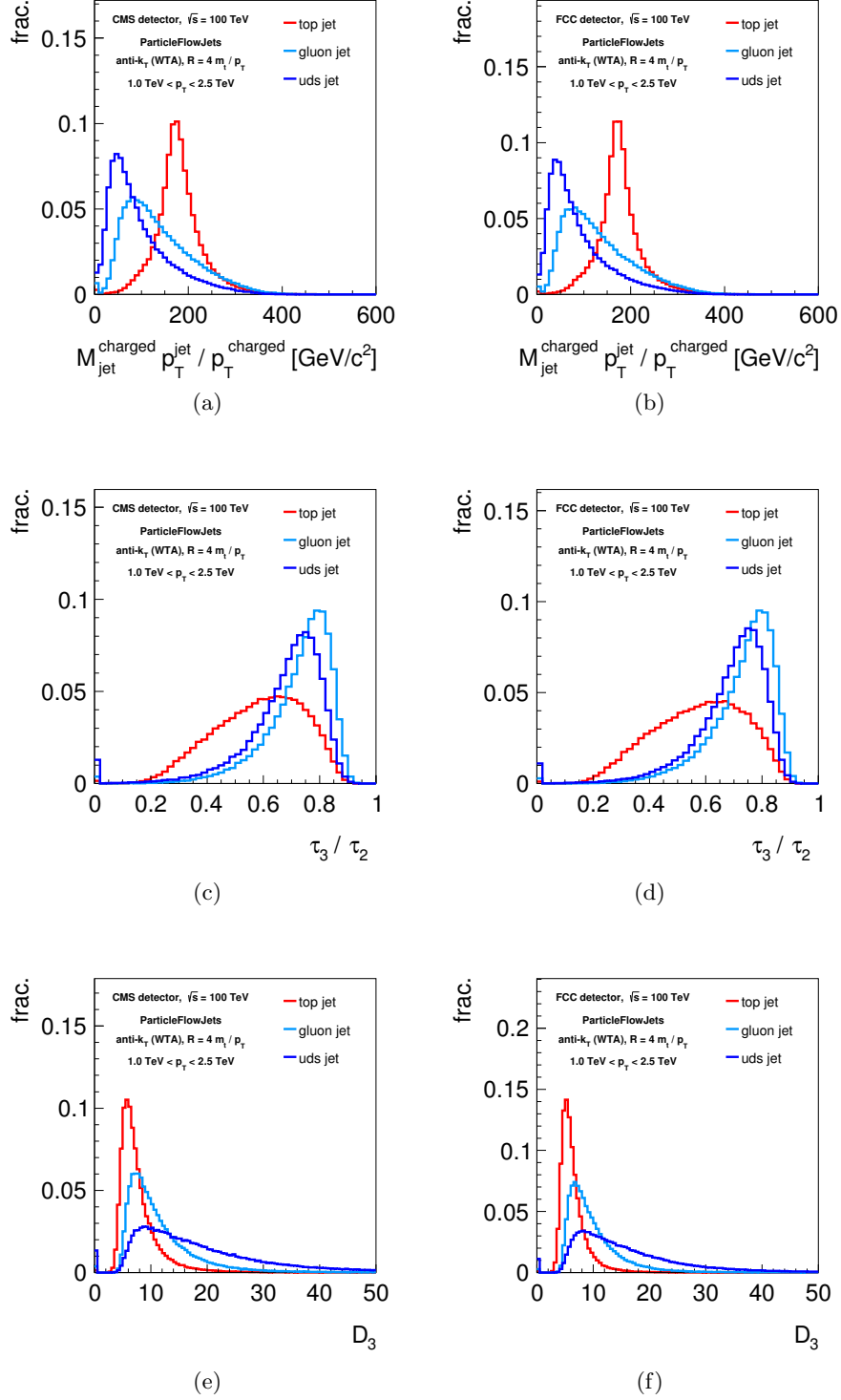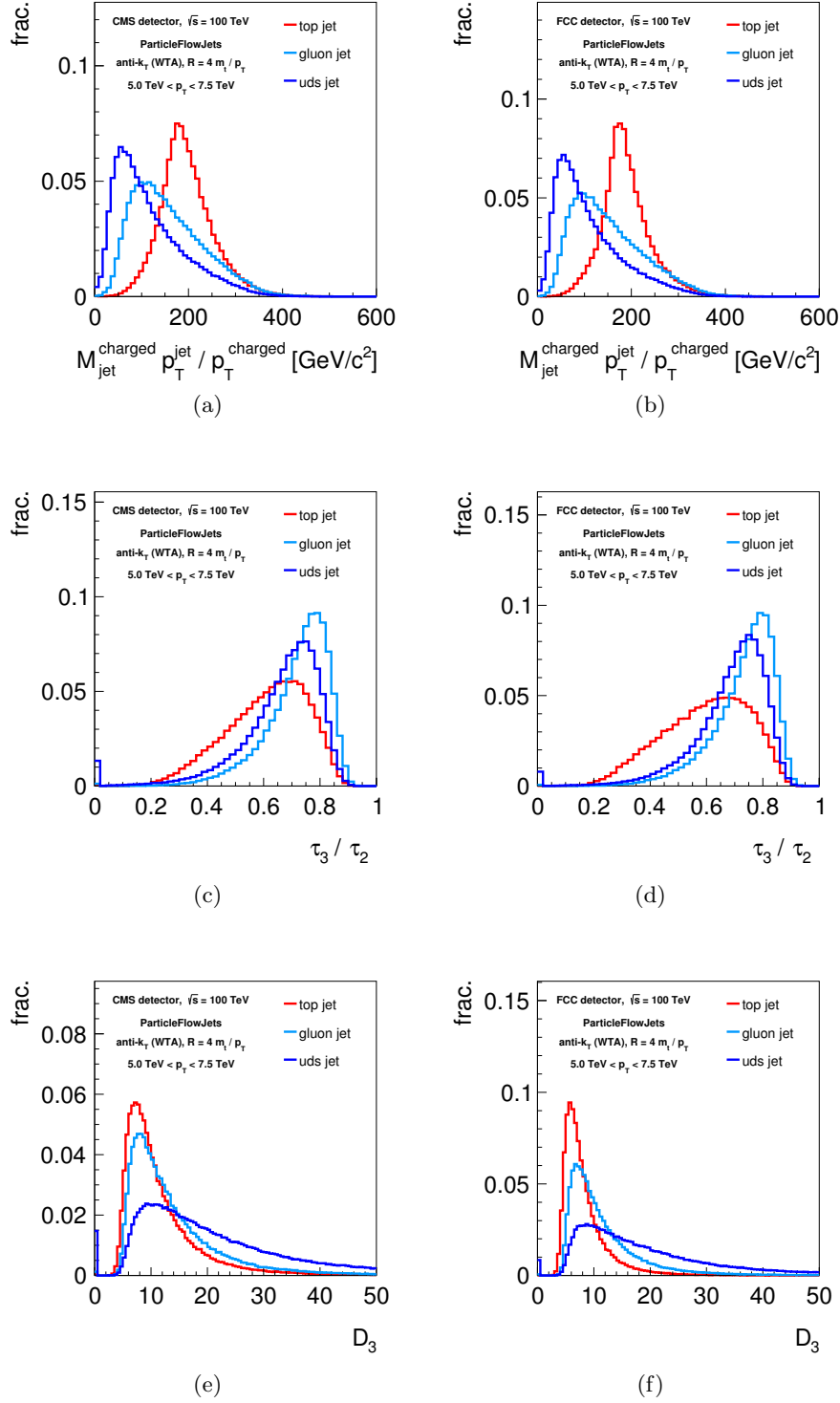
Figure 11: Distributions of the jet mass (top), τ_3/τ_2 (middle), and D_3 (bottom) as measured on anti-k_T jets with radius $R = 4m_{\text{top}}/p_T$ and $p_T \in [5.0, 7.5]$ TeV on boosted top jets and QCD jets from light quarks and gluons. (left) Distributions as measured from the CMS detector's calorimeter system. (right) Distributions as measured from a future collider detector's calorimeter system.
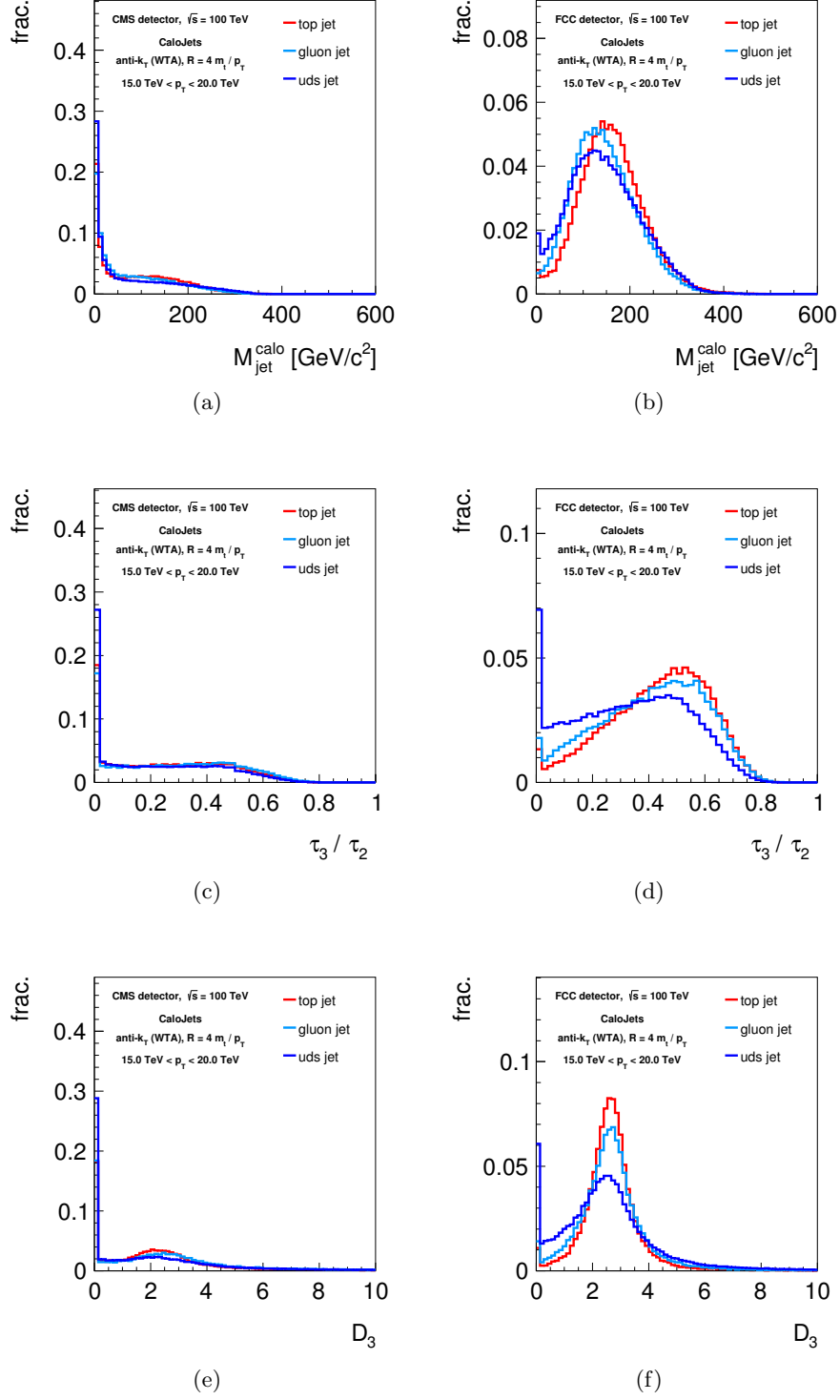
Figure 12: Distributions of the jet mass (top), τ_3/τ_2 (middle), and D_3 (bottom) as measured on anti-k_T jets with radius $R = 4m_{\text{top}}/p_T$ and $p_T \in [15, 20]$ TeV on boosted top jets and QCD jets from light quarks and gluons. (left) Distributions as measured from the CMS detector's calorimeter system. (right) Distributions as measured from a future collider detector's calorimeter system.
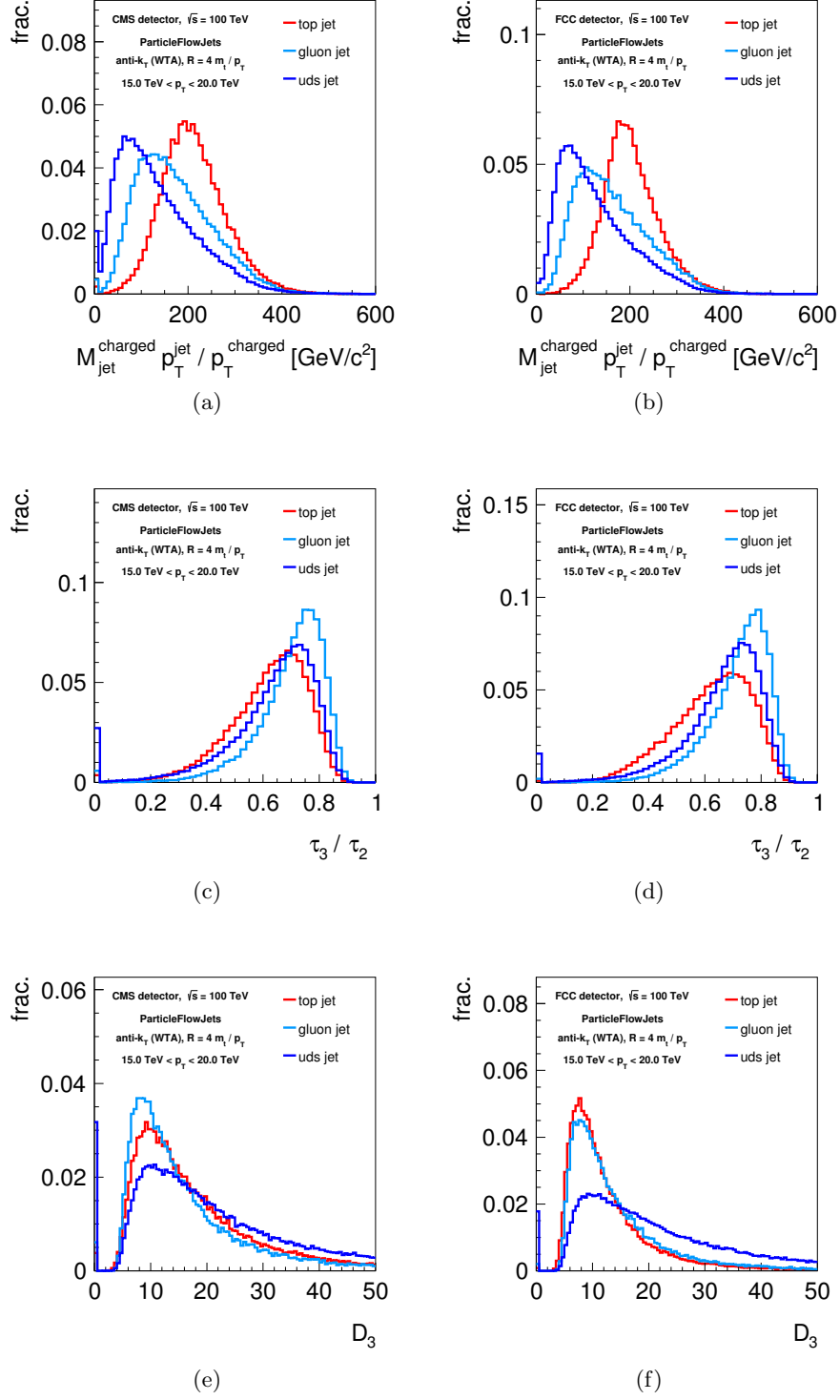
Figure 13: Distributions of the rescaled track-based jet mass (top), τ_3/τ_2 (middle), and D_3 (bottom) as measured on anti-k_T jets with radius $R = 4m_{\text{top}}/p_T$ and $p_T \in [1.0, 2.5]$ TeV on boosted top jets and QCD jets from light quarks and gluons. (left) Distributions as measured from the CMS detector's tracking system. (right) Distributions as measured from a future collider detector's tracking system.

Figure 14: Distributions of the rescaled track-based jet mass (top), τ_3/τ_2 (middle), and D_3 (bottom) as measured on anti-k_T jets with radius $R = 4m_{\text{top}}/p_T$ and $p_T \in [5.0, 7.5]$ TeV on boosted top jets and QCD jets from light quarks and gluons. (left) Distributions as measured from the CMS detector's tracking system. (right) Distributions as measured from a future collider detector's tracking system.

Figure 15: Distributions of the rescaled track-based jet mass (top), τ_3/τ_2 (middle), and D_3 (bottom) as measured on anti-k_T jets with radius $R = 4m_{\text{top}}/p_T$ and $p_T \in [15, 20]$ TeV on boosted top jets and QCD jets from light quarks and gluons. (left) Distributions as measured from the CMS detector's tracking system. (right) Distributions as measured from a future collider detector's tracking system.
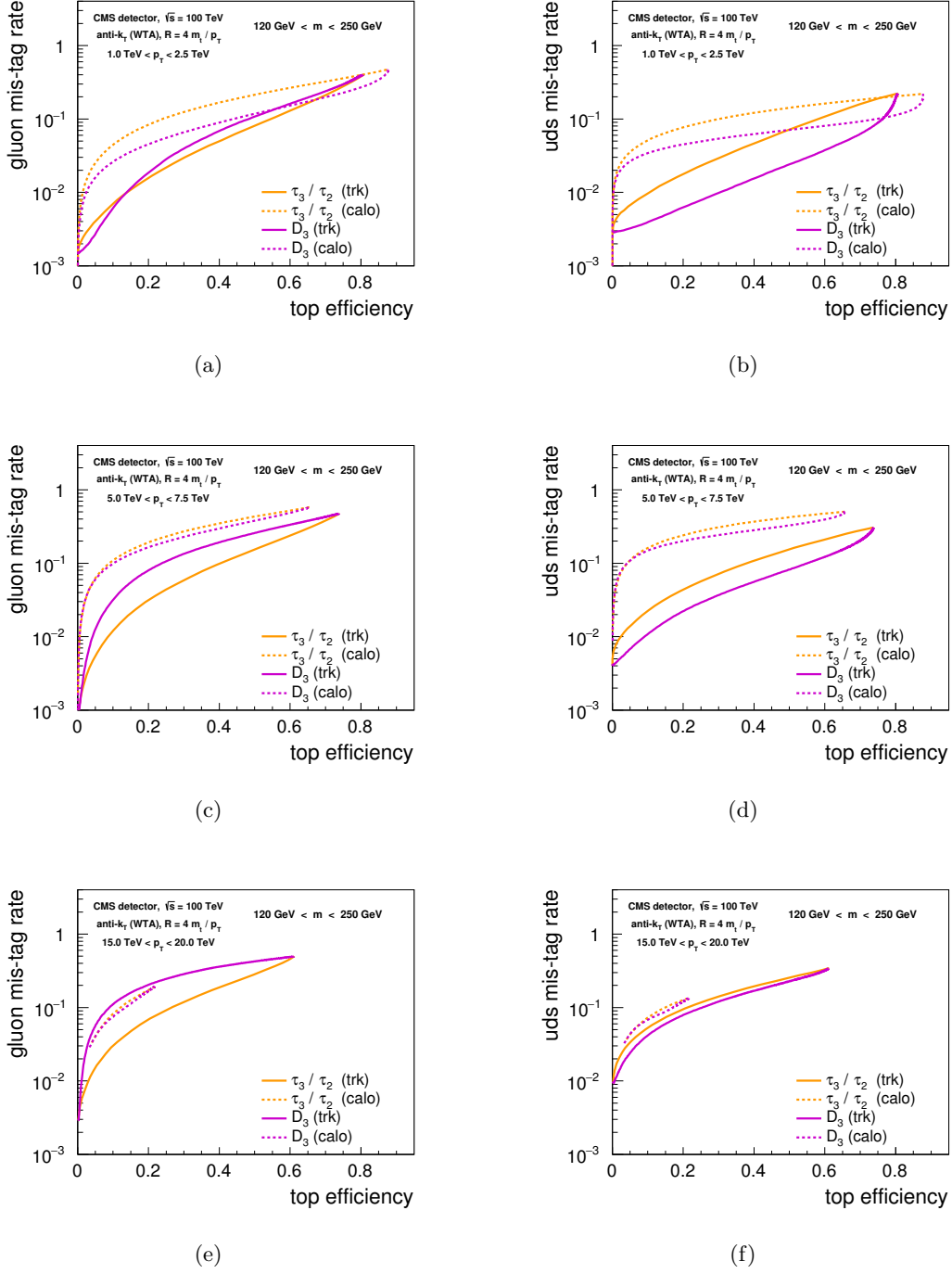
Figure 16: Signal vs. background efficiency (ROC) curves for top quark identification from QCD background utilising $\tau_{3,2}$ and D_3 with the CMS detector for three p_T bins: $[1.0, 2.5]$ TeV (top), $[5.0, 7.5]$ TeV (middle), $[15, 20]$ TeV (bottom). (left) top quarks vs. gluon jets, (right) top quarks vs. light quark jets. The cut on the jet mass of $m \in [120, 250]$ GeV is included in the efficiencies.
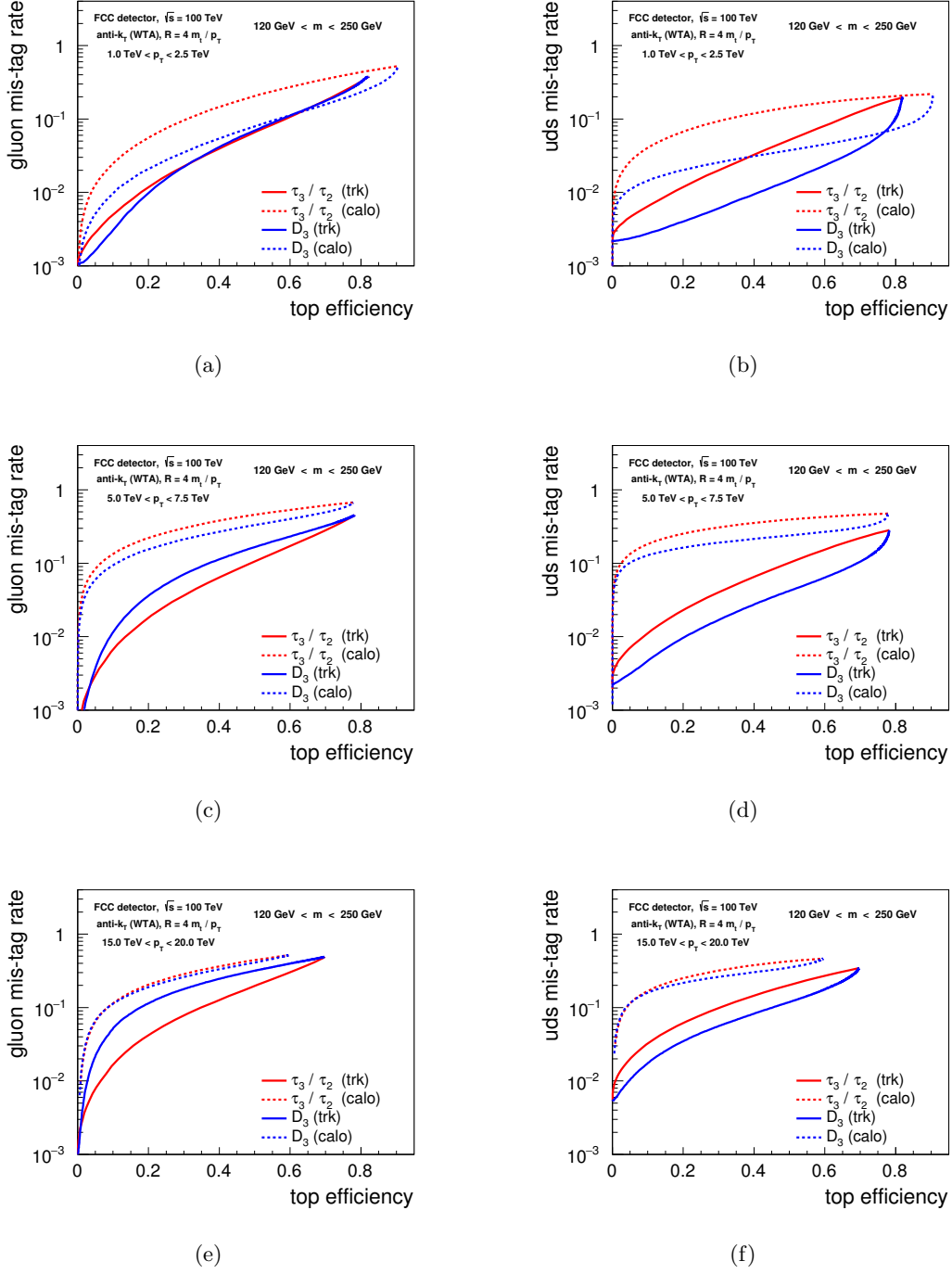
Figure 17: Signal vs. background efficiency (ROC) curves for top quark identification from QCD background utilising $\tau_{3,2}$ and D_3 with the FCC detector for three p_T bins: $[1.0, 2.5]$ TeV (top), $[5.0, 7.5]$ TeV (middle), $[15, 20]$ TeV (bottom). (left) top quarks vs. gluon jets, (right) top quarks vs. light quark jets. The cut on the jet mass of $m \in [120, 250]$ GeV is included in the efficiencies.